Deep-Sea Research II 58 (2011) 2678–2694

Contents lists available at ScienceDirect

Deep-Sea Research II

journal homepage: www.elsevier.com/locate/dsr2

Dissolved iron in the Southern Ocean (Atlantic sector)

M.B. Klunder [a,*], P. Laan [a], R. Middag [a], H.J.W. De Baar [a,b], J.C. van Ooijen [a]

[a] Royal Netherlands Institute for Sea Research (Royal NIOZ), P.O. Box 59, 1790 AB, Den Burg, Texel, The Netherlands
[b] Department of Ocean Ecosystems, University of Groningen, Groningen, The Netherlands

ARTICLE INFO

Article history:
Received 21 October 2010
Accepted 21 October 2010
Available online 3 December 2010

Keywords:
Iron
Hydrothermal
Upwelling
Sea-ice
Dust
Antarctic
Southern Ocean
Antarctic Circumpolar Current
Weddell Gyre

ABSTRACT

We report a comprehensive dataset of dissolved iron (Fe) comprising 482 values at 22 complete vertical profiles along a 1° latitudinal section at the Zero meridian. In addition a shorter high resolution (~00°09′) surface section of the southernmost part of the transect (66°00′–69°35′S) is presented. Within the upper surface mixed layer the concentrations of dissolved Fe vary between 0.1 and 0.3 nM. An inverse trend versus fluorescence suggests significant Fe removal by plankton blooms. Vertical mixing and upwelling are the most important supply mechanisms of iron from deep waters to the upper surface mixed layer. At lower latitude (42°S) there is a distinct maximum of 0.6–0.7 nM in the 2000–3000 m depth range due to inflow of North Atlantic Deep Water. In one region (55°S) elevated dissolved Fe found in the surface mixed layer is ascribed to the recent deposition of aeolian dust originating from South America. Close to the Antarctic continent there is an indication of Fe supply in surface waters from icebergs. In the deep waters there is a strong indication of a hydrothermal plume of dissolved Fe and Mn over the ridge in the Bouvet region (52–56°S). In the Weddell Gyre basin the dissolved Fe in the deep water is 0.47 ± 0.16 nM in the eastward flow at ~56–62°S and is lower with a value of 0.34 ± 0.14 nM in the westward flow at high ~62–69°S latitude. At the edge of the continental ice-sheet on the prime meridian, the continental margin of the Antarctic continent appears to be lesser source of dissolved Fe than in any other place in the world; this is likely because it is unique in being overlain by the extending continental ice-sheet that largely prevents biogeochemical cycling.

1. Introduction

Dissolved Fe has been recognized to be a key element for phytoplankton growth in the world oceans (Coale et al., 1996). It is needed for important biological processes such as photosynthesis and is used in several enzymes (Sunda, 2001). Although Fe is the fourth most abundant element in the earth crust, it is only available in trace concentrations (generally <1 nM) in the oxygenated water of the world oceans (De Baar and De Jong, 2001). In the Southern Ocean, the presence of ample major nutrients (N,P, and Si) yet low phytoplankton abundance has been hypothesized to be due to the lack of this essential trace nutrient (Gran, 1931; Hart, 1934, 1942; Martin, 1988) in combination with low light conditions (Sunda and Huntsman, 1997). This was first confirmed in bottle incubations by De Baar et al. (1990) and Buma et al. (1991), and since then has been verified by others—see review by De Baar and Boyd (2000). During *in situ* Fe fertilization experiments the effect of extra Fe was shown repeatedly; however the light limitation effect of deep Surface Mixed Layers due to high wind velocity also plays a key role (see reviews by De Baar et al., 2005; Boyd et al., 2007). More recently natural Fe fertilization was reported over shallow plateau regions around subantarctic islands (Blain et al., 2007; Pollard et al., 2009).

Because of the low concentration of dissolved Fe in open ocean waters, the sampling, filtration and analysis are very sensitive to contamination. As a result the world ocean dataset of dissolved Fe in the published literature is quite small in number of datapoints and in geographical and vertical distribution, notably in the Southern Ocean.

Recently, more ocean datasets of dissolved Fe have become available in the Southern Ocean (Sedwick et al., 1997, 2008; Sohrin et al., 2000; Boye et al., 2001; Measures and Vink, 2001; Croot et al., 2004; Nishioka et al., 2005; Planquette et al., 2007; Blain et al., 2008a; Lai et al., 2008), and elsewhere (Bell et al., 2002; Laës et al., 2003, 2007; Sarthou et al., 2003; Boyle et al., 2005; Measures et al., 2008). Recent world ocean data compilations have also been made (Gregg et al., 2003; Parekh et al., 2004; Moore and Braucher, 2008) and include Fe values in the Southern Ocean. Nevertheless, determination of the concentration and basin wide gradients of dissolved iron in the deep ocean basins remains a challenge in oceanography, mainly in the (less studied) deep Southern Ocean.

With the purpose of addressing this issue, two new developments have allowed major progress in sampling trace metals over the recent years. Firstly, a new ultra clean sampling system has been developed and successfully tested (De Baar et al., 2008)

* Corresponding author. Tel.: +31 222 369 459.
E-mail address: Maarten.klunder@nioz.nl (M.B. Klunder).

0967-0645/$ - see front matter © 2010 Elsevier Ltd. All rights reserved.
doi:10.1016/j.dsr2.2010.10.042

(see Section 2), allowing faster and more reliable clean sampling at higher resolution, of specifically the deep waters. Secondly, international exercises (Bowie et al., 2003, 2006; Johnson et al., 2007) have eventually led to the availability of certified reference samples of dissolved Fe in seawater.

Several sources of dissolved Fe to the Southern Ocean can be envisioned. The Fe in surface waters may come from above by dust input originating from adjacent continental source regions, notably Patagonia (South America), South Africa and Australia (Jickells and Spokes, 2001; Sedwick et al., 2008). Alternatively Fe may come from below by upwelling and upward mixing of deeper waters containing higher dissolved Fe than the surface waters (Löscher et al. 1997; Croot et al., 2004; Lai et al., 2008). Obviously the deep waters would in turn need a source as well, where reductive dissolution within suboxic marine sediments and remineralization of particles are known sources of Fe (De Baar and De Jong, 2001) and Mn (Froelich et al., 1979). Hydrothermal vents at active mid-ocean ridges are another known source of dissolved Fe and Mn (Klinkhammer et al., 2001). The parallel determination of dissolved Mn (Middag et al., 2011) may provide clues as to these source terms. Finally in the polar oceans, meltwater from the continental Antarctic ice-sheet continuously flows into the sea where some of its Fe contents may become dissolved. Moreover, icebergs broken off from the ice-sheet often become temporarily grounded on the shelf and entrain dirt hence Fe from the shelf sediments (Löscher et al., 1997). Finally, the seasonal sea-ice also comprises some Fe (Lannuzel et al., 2008) which upon melting may contribute to the Fe content of the surface waters.

Here we present the distribution of dissolved Fe at a high resolution (1° latitude) transect (Fig. 1) over the complete 4–5 km depth of the water column, overall 482 dissolved Fe values at 22 stations with 20–24 sample depths. This section is designed across the Antarctic Circumpolar Current (ACC) as to be representative of the ACC flowing all around Antarctica. Moreover the southernmost part of the section represents the eastern extent of Weddell Gyre. Within the Weddell Gyre, an additional small set of 24 samples for dissolved Fe was collected in the very same surface waters from 66°02.18′S–69°35.15′S by deployment of a towed fish so as to obtain high (~00°09′) resolution surface water concentrations. This sampling scheme allowed us to accurately determine the distribution of dissolved iron, and establish its sources in the Atlantic sector of the Southern Ocean.

2. Materials and methods

2.1. Sampling

2.1.1. Vertical profile sampling

Seawater samples were collected during the ANT XXIV/3 expedition of the R.V. Polarstern (Cape Town to Punta Arenas: 10 February until 14 April 2008) on its first transect from Cape Town to the Antarctic ice-sheet of Antarctica (Fig. 1). Here, in total 22 stations were sampled for analyses of dissolved Fe and other trace metals (see Section 2.4). On the prime meridian transect, the resolution is typically 1°, except for a station at 66°30.06′S instead of ~66°S and the southernmost station at 69°24.03′S close to the approximately 200 m thick ice-sheet extending beyond the Antarctic continent over the shelf seas.

All bottles used for storage of reagents and samples were cleaned according to an intensive three step cleaning protocol extensively described by Middag et al. (2009). Samples were taken using 24 internally Teflon-coated PVC 12 l GO-FLO Samplers (General Oceanics Inc.) mounted on a Titanium frame which was connected to a Kevlar hydrowire with internal signal cables for data transfer and control from the ship. Directly upon recovery the complete frame with samplers was placed inside a class 100 clean container (De Baar et al., 2008). Seawater was filtered in line over a 0.2 μm filter cartridge (Sartrobran-300, Sartorius) under 1.5 bar nitrogen pressure. Before seawater collection, the first 0.5 l. of seawater was filtered and disposed for rinsing purposes. Two (one for measuring, one for back-up) LDPE sample containers (NALGENE, 60 ml) were filled from each GO-FLO sampler for analyses of dissolved Fe.

2.1.2. Surface water sampling

In the Weddell Gyre, close to the Antarctic continent 24 additional samples were collected along the southernmost part of the transect (66°02.18′S–69°35.15′S) using a towed epoxy-coated stainless steel torpedo deployed off a crane arm on the starboard side of the ship, after De Jong et al. (1998). In between vertical sampling stations, a seawater sample was collected every hour, and was analyzed as described in Section 2.5. Due to differences in ship speed this resulted in a slightly unequal resolution of 00°09′ on average.

2.2. Analysis of Fe

2.2.1. Chemicals

A solution of 0.4 M hydrochloric acid was made by diluting 30% concentrated HCl (Merck, suprapur, 10 M), 0.35 M H_2O_2 solution by dilution of 30% H_2O_2 (Merck, suprapur) and the 0.96 M NH_4 solution was made from 25% NH_4OH (Merck, suprapur). A luminol stock solution was prepared by dissolving 270 mg luminol (3-aminophtalhydrazide, Aldrich) and 500 mg potassium hydroxide in 15 ml Milli-Q (MQ) water (MQ water is defined as ultrapure water with resistance $\geq$ 18.2 MΩ). To prepare the final reagent used in this system 3 ml of luminol stock solution and 60 μl triethylenetetramine (TETA) (Merck) were diluted in 1 l of MQ. The 0.12 M ammonium acetate buffer (pH=6.5) was made by diluting a 2.0 M buffer solution. This 2.0 M buffer solution was obtained by a tenfold dilution of a saturated solution of ammonium acetate crystals after Aguilar-Islas et al. (2006).

2.2.2. Method

The shipboard analysis method used is by Flow Injection—Chemiluminescence method with preconcentration on iminodiacetic acid (IDA) resin as described by De Baar et al. (2008), with some minor modifications. One modification is the initial acidification of the samples; here the samples were acidified to pH=1.8 by adding 120 μl/60 ml sample (2‰) of ultraclean HCl (12 M) (Seastar Baseline®Hydrochloric Acid, Seastar Chemicals) and left for at least 12 h before analyzing.

The method detects Fe (III). Here, we ensured that all the Fe was in the Fe (III) form, by adding 60 μl of a 1‰ hydrogen peroxide (Merck suprapur 30%) solution at least 1 h before measuring as recommended by Johnson et al. (2007).

All samples from one station were measured within one run, from surface to deep and each sample analyzed in triplicate as follows. Each sample was buffered in-line to pH=4.0 by mixing it with a 0.12 M acetate buffer (pH=6.5). After buffering, the sample passed over a chelating iminodiacetic acid (IDA, Toyopearl, AFChelate 650 M)) column for 120 s. The column was rinsed by flow-through of MQ for 1 min before the Fe was eluted with 0.4 M HCl (Merck suprapur). A four port selection valve (VICI, Switzerland) was used for switching between buffer/sample and MQ passing over the IDA—preconcentration column.

The eluent was mixed with 0.96 M ammonia, 0.35 M hydrogen peroxide and the luminol solution. The mixture passed through a 5 m length mixing coil in a constant 35 °C water bath, before injection in a Hamamatsu (HC 135) photon counter. This injection step took 180 s.

A six port injection valve (VICI, Switzerland) was used to switch between inflow of sample, rinsing MQ over the column and elution

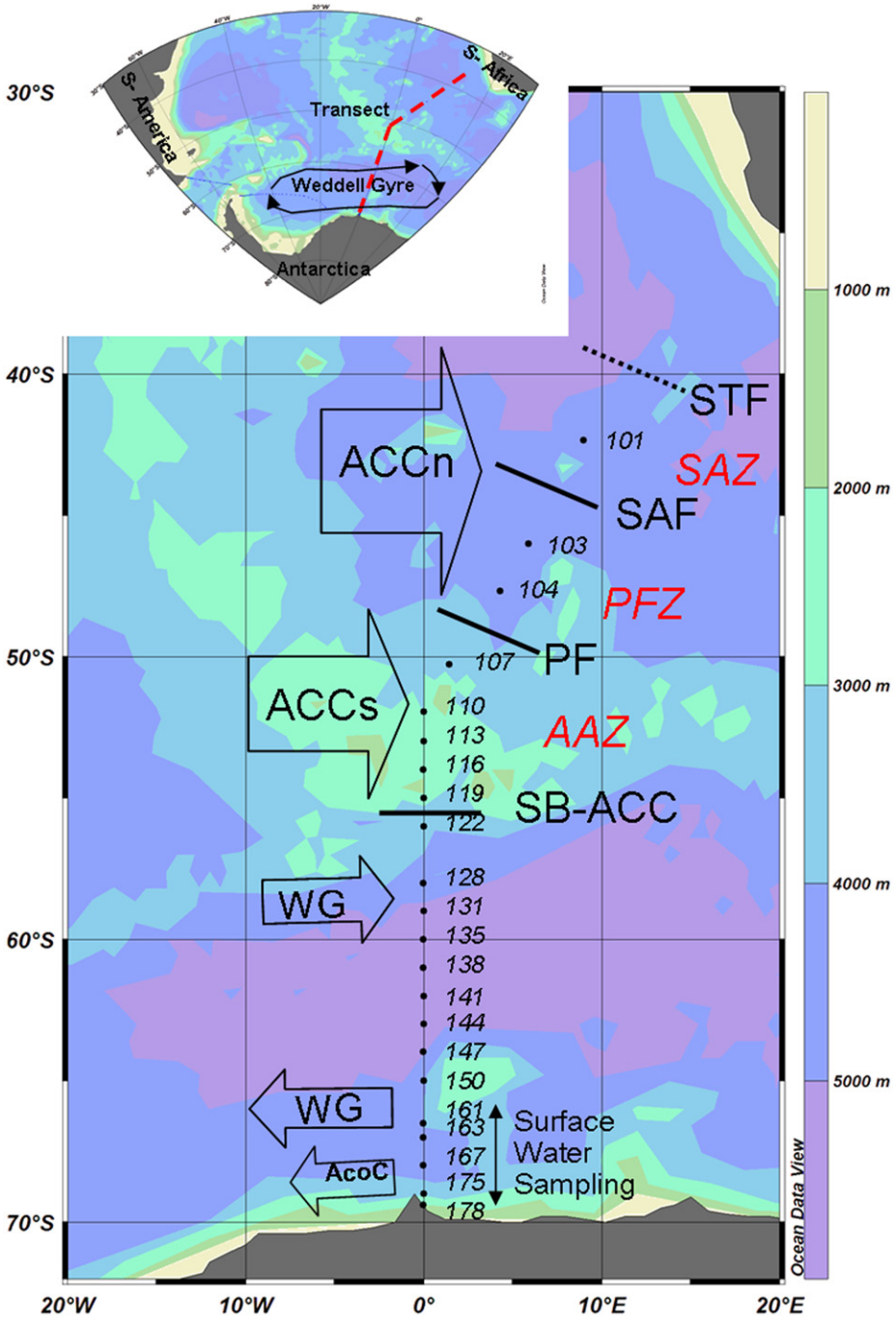

Fig. 1. Research area with station positions. Presented are all stations sampled for trace metals during the ZERO meridian transect of ANT XXIV/3, including station numbers for sampling with the ultraclean Titanium frame. Not shown are other stations in between (i.e. the missing numbers) where additional data of major nutrients and other variables was collected with a regular CTD/Rosette. Also, the ~66 to 69.30′°S region where the towed fish is deployed for Surface Water Sampling is shown. Depth isolines are shown as well as fronts (normal, black), zones (italic, red) and major currents (arrows). Abbreviations in alphabetical order: AAZ: Antarctic Zone; ACCn: Antarctic Circumpolar Current northern branch; ACCs, Antarctic Circumpolar Current southern branch; ACoC: Antarctic Coastal Current; PF: Polar Front; PFZ: Polar Front Zone; SAF: Subantarctic Front; SAZ: Subantarctic Zone; SB-ACC: Southern Boundary of the ACC; STF: SubTropical Front (dotted line, its position not sampled nor defined in our cruise); WG: Weddell Gyre. The inset shows the sampling transect (red) in a regional context, also the Weddell Gyre is indicated. This figure is made using Ocean Data View (Schlitzer, 2009).

by HCl. The autosampler valve, both switching valves and the detector were controlled by an interface developed in LabView™.

The system was calibrated for every run using standard additions (0.1–1.5 nM range) of an 895.5 nM Fe stock solution to filtered seawater obtained from the subsurface minimum, with lowest Fe concentrations. This calibration seawater was taken for each station at the depth of the chlorophyll maximum. Concentrations varied between 0.05 nM (station 163) and 0.25 nM (station 138). The stock solution was obtained by dilution of a 1000 ppm ICP-MS standard (Fluka Chemicals).

2.3. Blank, limit of detection and validation

Regularly the combined blank of the 1 min MQ-column wash and the 0.4 M HCl for elution of the column was calculated from the

amount of counts measured upon zero (0) s loading time. The average value for this blank was 32 ± 14 pM Fe ($n=19$) and this blank did not exceed 60 pM. By double versus single addition of the H_2O_2 it was found that this did not cause a blank. The contribution of the Seastar Baseline®Hydrochloric Acid is deemed to be negligible (< 0.04 pM/sample).

The detection limit was determined regularly and defined as the standard deviation of 5 peaks of 10 s loading of low-Fe seawater (subsurface minimum), multiplied by 3. Average detection limit was typically 5.7 ± 2.9 pM Fe ($n=4$), and the detection limit did not exceed 8.5 pM Fe.

In order to validate the accuracy of the system, standard reference seawater was measured regularly, also in triplicate. This water was obtained during the preceding SAFe-cruise in 2004 and has since then proven to be of great value for validation of on-board Fe measurements (Johnson et al., 2007). There is SAFe surface (S) water and SAFe deep (D2) water available to validate against different ranges of Fe concentration. The average value of the SAFe S waters we found was 0.13 ± 0.021 nM Fe ($n=11$) for our analysis, compared to the community consensus value of 0.097 ± 0.43 nM. However, a small difference between different SAFe S bottles appears to influence the results. Obtained concentrations of 0.16 ± 0.01 nM Fe ($n=3$) for bottle S-391 and 0.172 nM for bottle S-135 ($n=1$) elevate our results for SAFe S calibration water. When excluding latter bottles S-391 and S-135 the average value of SAFe-S waters we found was 0.11 ± 0.012 ($n=7$). For the SAFe deep (D2) inter calibration waters we found an average value of 0.96 ± 0.06 nM Fe ($n=10$), consistent with the community consensus value of 0.91 ± 0.17 nM (Johnson et al., 2007).

2.4. Other parameters

Samples for dissolved manganese (Mn) and aluminium (Al) and Zinc (Zn) were taken from the same Titan system, and results reported by Middag et al. (2011a, b) and Croot et al. (2011), respectively. Also major nutrients (silicate, nitrate and phosphate) were measured from samples from the Titan system, as well as at in-between stations using a standard CTD/Rosette system. Salinity (conductivity), temperature and pressure (depth) were measured using the CTD system (Seabird SBE 911+) mounted in the titanium frame. This CTD system also included a Chelsea MK-III fluorometer, for measurements of fluorescence (arbitrary units). Another CTD/Rosette with regular samplers was deployed at in-between stations and did provide vertical light transmissometry records indicative of the abundance of suspended particles.

The meteorological parameters, including precipitation, were measured regularly by the shipboard staff of the German Meteorological Service. Underway salinity and temperature were measured every ten seconds at a depth of 5 m using an instrument operated by the company FIELAX. Synoptic sea-ice and ice-berg data were registered on board by dedicated ice-watch person on the bridge.

2.5. Database

The complete database of dissolved Fe and ancillary variables is available in the electronic supplement www.deepsearesearch.com. An overall 508 data values of dissolved Fe are listed, among which 482 values are used in this manuscript. Another 26 values (5.1% of the total dataset) are flagged as (suspect) outliers. These 26 outliers were not used in figures and in the interpretation of this manuscript. The criteria for rejection are based on the comparison with other parameters measured from the same GO-FLO sampler, and curve fitting versus samples collected above and below the suspect sampler. The criteria for the rejection of values are described in the online supplementary material. The complete relational database will be available at the international GEOTRACES datacentre (http://www.bodc.ac.uk/geotraces/).

3. Results

3.1. Hydrography and major nutrients

The hydrography with major fronts, zones and currents (as described in the online electronic supplement) is shown schematically in Fig. 1. Along the complete vertical section the different water masses and the depth of the Surface Mixed Layer are shown in Fig. 2. Throughout the section the distinct surface layer with uniform potential density represents the Surface Mixed Layer (SML). The depth of this Surface Mixed Layer (Table 1) varied between 28 and 124 m and was typically ~100 m deep from station 101 (~42°20′S) to station 128 (~58°S), and was 25–50 m deep from stations 131 to 175 (~59–69°S). On average the SML depth was ~65 m.

The distributions of nitrate and silicate along the section are shown in Fig. 3. The distribution of phosphate is similar to that of nitrate (here not shown, see graph S-1 in online electronic supplement).

In the surface waters of the Subantarctic Zone at the northernmost station 101 (Fig. 4) there is ample nitrate at ~15 μM. Going further southward the nitrate in surface waters further increases (Fig. 3) to about 26 μM (Fig. 4 stations 113 and 167) which is the typical summer value in the Southern Ocean, due to seasonal depletion by biological uptake with about 6 μM versus the winter water at typical 32 μM. The trends for phosphate (not shown) are similar as for nitrate, increasing from 1.04 μM (station 101) to the typical summer value of about 1.7 μM (stations 113 and 167). Thus at all stations phosphate and nitrate conditions were non-limiting

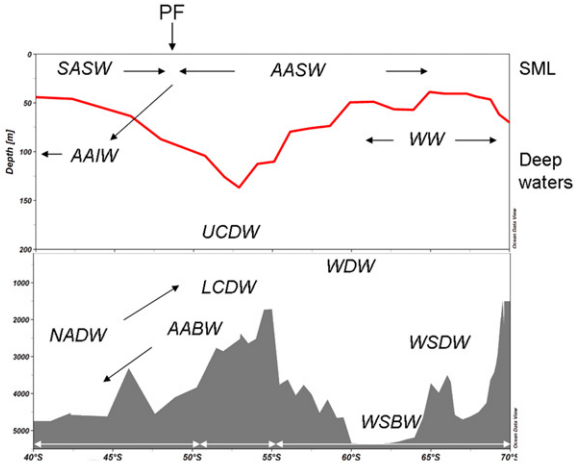

	SubAntarctic Region	Bouvet Region	Weddell Gyre
SML	0.24 +/- 0.06 (n=17)	0.24 +/- 0.13 (n=21)	0.19 +/- 0.09 (n=26)
Deep Water	0.40 +/- 0.12 (n=61)	0.61 +/- 0.40 (n=84)	0.39 +/- 0.15 (n=251)

Fig. 2. Schematic overview of the transect with above the upper 200 m and below the 200–5500 m depth range. The red line indicates the depth of the Surface Mixed Layer (SML). Water masses as further described in the online supplement are as follows: SASW: SubAntarctic Surface Water; AASW: Antarctic Surface Water; WW: Winter Water; AAIW: Antarctic Intermediate Water; Upper Circumpolar Deep Water; NADW: North Atlantic Deep Water; LCDW: Lower Circumpolar Deep Water; WDW: Warm Deep Water; AABW: Antarctic Bottom Water; WSDW: Weddell Sea Deep Water; WSBW: Weddell Sea Bottom Water. Below the graph the average Fe concentration (average, standard deviation, n) is reported for both the SML and the Deep Water in the three distinct regions of the transect. This figure is made using Ocean Data View (Schlitzer, 2009).

Table 1
Mixed layer depths, SML average values for Fe and fluorescence and 25 m average values for Fe and Al.

Station	Latitude (°S)	SML depth (m)	Surface mixed layer average		Upper 25 m average	
			Fe (nM)	Fluoresence	Fe (nM)	Al (nM)
101	42.34	46	0.28	0.41	0.30	0.85
103	46.00	65	0.22	0.65	0.26	1.33
104	47.66	80	0.19	0.42	0.17	0.62
107	50.27	95	0.21	0.29	0.18	0.62
110	51.95	124	0.11	0.32	0.18	0.61
113	53.00	133	0.18	0.31	0.15	0.56
116	54.00	102	0.29	0.14	0.33	1.14
119	55.00	95	0.33	0.10	0.47	1.78
122	56.00	77	0.34	0.14	0.41	0.75
128	58.00	73	0.18	0.23	0.18	0.53
131	59.00	67	0.13	0.11	0.17	0.61
135	60.01	40	0.24	0.16	0.27	0.35
138	61.00	42	0.25	0.19	0.25	0.32
141	62.00	47	0.27	0.31	0.27	0.52
144	63.00	47	0.23	0.30	0.23	0.82
147	63.97	28	0.32	0.26	0.32	1.46
150	65.00	33	0.16	0.70	0.16	0.57
161	66.50	32	0.23	0.63	0.23	1.40
163	67.00	39	0.15	1.16	0.15	0.36
167	68.00	42	0.10	1.29	0.08	0.35
175	69.00	45	0.13	1.68	0.13	0.20
178	69.40	67	0.32	1.60	0.34	0.64

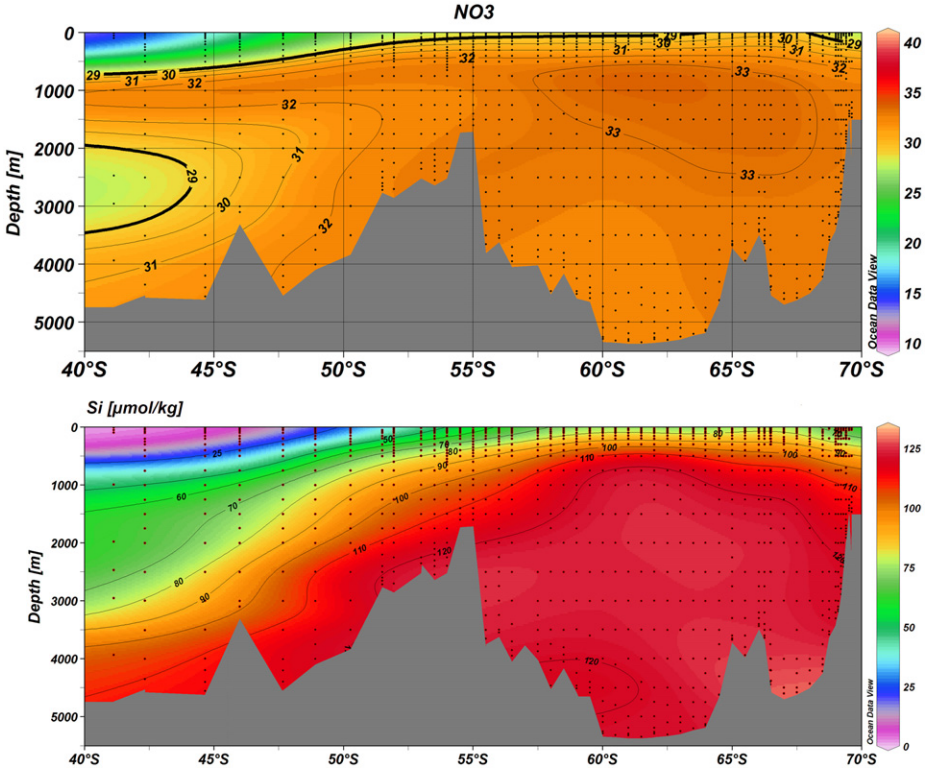

Fig. 3. Color and contour plots of the concentration (µmol/kg) of nitrate (upper graph) and silicate of the transect. Due to extra hydrocasts with regular CTD/Rosette there are more individual datapoints (dots) than in Fig. 5 for dissolved Fe. This figure is made using Ocean Data View (Schlitzer, 2009).

for phytoplankton growth. The silicate is found to be depleted at 0.5 µM at station 101 (Fig. 4A), then slowly increases southward (Fig. 3) to 0.9 µM (station 103), 1.9 µM (station 104), thus less than the common 1 µM criterion for conceivable limitation of large diatoms. Across the Polar Front the silicate shows the well-known steep rise to the maximum surface value of 68 µM (station 130, not shown) and then slightly decreases again to 51 µM (not shown) at southernmost station 178 near the continental ice-sheet. These surface waters show low summer values of silicate and nitrate coinciding with temperature stratification (Fig. 4, see inset graphs of station 113 and station 167). An improved more stable light climate due to summer stratification has most likely favored diatom growth (De Baar et al., 2005) in the preceding months before our sampling, however there still is ample nitrate and

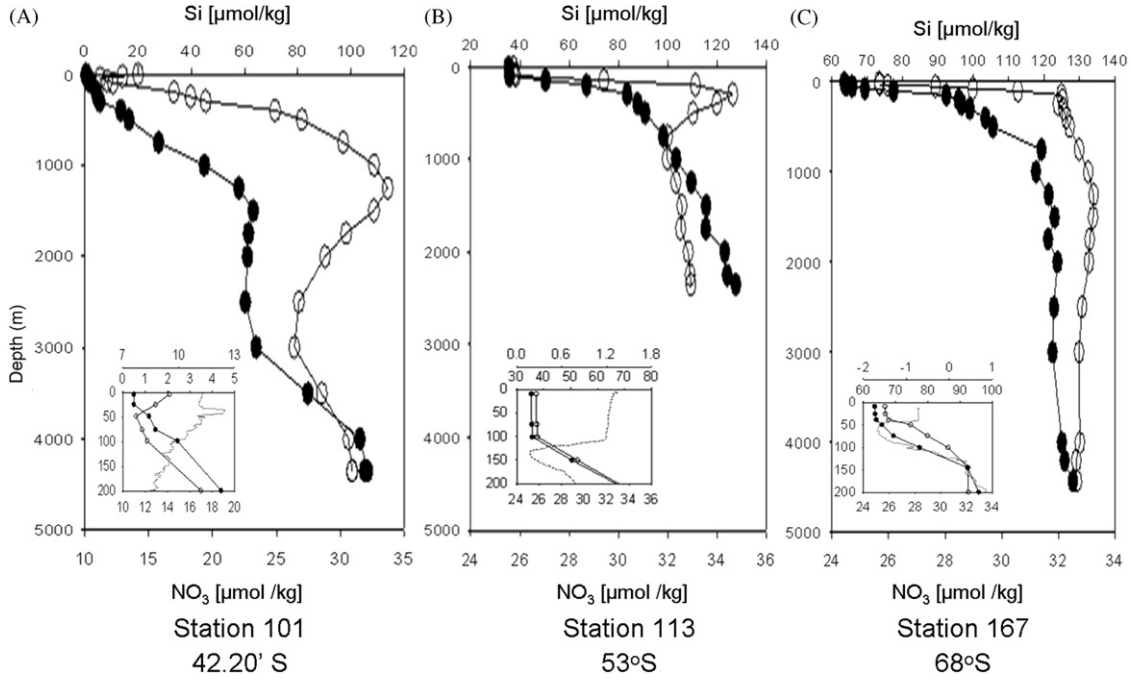

Fig. 4. Depth profiles of silicate (full circle) and nitrate (empty circle) of station 101 (A), station 113 (B) and station 167 (C) as indicative of three distinct regions (see text). Insets in each graph show the upper 200 m at expanded scales of silicate and nitrate (horizontal; µM) and depth (vertical), as well as potential temperature (dotted line) with additional scales (ranging from 7 to13 °C, 0 to 1.8 °C and −2 to 1 °C) along the horizontal axis.

silicate available. Here the combination of limitation by light with Fe deficiency is deemed limiting for phytoplankton growth (De Baar et al., 1990, 1995, 2005).

In the deep waters the more saline NADW coming from the north and rising southwards is easily recognized by the relatively low nitrate in the 2000–3000 m depth range as marked by the black contour drafted at 29 µM (Fig. 3). This nitrate minimum is also visible in the vertical profiles of nitrate at station 101 (Fig. 4A) where in the same 2000–3000 m depth interval the silicate is uniform (and actually shows a slight minimum), as opposed to its typical steady increase with depth (station 113) elsewhere along the section and in the world oceans.

3.2. General distribution of dissolved Fe throughout the water column

Along the complete section (Fig. 5) the dissolved Fe is depleted in the surface waters (upper graph) in two regions at 46–52 and 66–69°S, respectively. In between there is station 119 at 55°S with elevated Fe in surface waters attributed to a recent aeolian dust input (see Section 4.1.1.2).

The deep waters (Fig. 5, lower graph) clearly show the elevated dissolved Fe in the NADW, where the Fe=0.55 nM contour (bold black line) more or less overlaps with the NO_3=29 µM contour (bold black line, Fig. 3). More southwards there is a strong Fe maximum over the Bouvet region attributed to hydrothermal input (see Sections 3.4.2 and 4.2.1.2). In this region, the Fe=0.6 nM contour (bold black line) strongly overlaps a similar Mn=0.3 nM contour also delineating the hydrothermal plume (Middag et al., 2011a). In contrast in the further southward Weddell Gyre the dissolved Fe becomes extremely low, with values decreasing from the eastward flowing branch (~60°S) to the westward flow (~66°S).

For the three distinct regions vertical profiles of dissolved Fe are shown in Fig. 6. All vertical profiles (Fig. 6) show a slight elevation in the surface (less clear at station 167), a subsurface minimum, and then low, slightly varying but increasing concentrations (<0.45 nM in the SubAntarctic region and Weddell Gyre, maximum 0.68 nM at 1000 m above the Bouvet region) until around 750–1000 m depth. In the SubAntarctic region, higher concentrations of ~0.5 to 0.6 nM occurred from 2000 to 3000 m, below which concentrations decreased until >0.4 nM (station 101, Fig. 6A). The stations over the ridge crest in the Bouvet region showed a different vertical profiles, with deep values >1 nM from 1200 m downwards and a maximum of 2.2 nM at 1750 m depth (station 116). In the Weddell Gyre the Fe concentrations were relatively constant at about 0.5 nM until the bottom (Fig. 6C, station 167).

For the three regions, the average dissolved Fe in the Surface Mixed Layer was 0.25 and 0.24 nM in the subAntarctic region and Bouvet region, respectively (Fig. 2), but significantly lower at 0.20 nM in the remote Weddell Gyre region, most notably in the westward flow at 66–69°S (Fig. 5, upper graph). In the deep waters the average dissolved Fe was significantly higher at 0.60 nM over the Bouvet region (Fig. 2) due to hydrothermal input as compared to 0.41 and 0.42 nM in the adjacent deep subAntarctic and deep Weddell Gyre regions, respectively.

3.3. Fe in the surface waters

3.3.1. Fe in the upper surface mixed layer

The surface waters were sampled in February and therefore represent the end of austral summer conditions. The upper surface concentration was measured at 10–25 m and was generally below 0.3 nM, except for stations 116 and 119 (54 and 55°S), where Fe concentrations were >0.4 nM.

The depth profiles of the Fe concentration showed a subsurface minimum at depths varying from 25 to 200 m. A significant decrease of this subsurface minimum was found from station 138 (61°S) (0.25 ± 0.01 nM) to station 175 (69°S) (0.05 ± 0.001 nM), with the strongest decline from station 161 (66°30′S) (0.16 ± 0.008 nM) southwards. Moreover, the depth of the subsurface minimum followed the latitude: deeper minima were found at the higher latitudes.

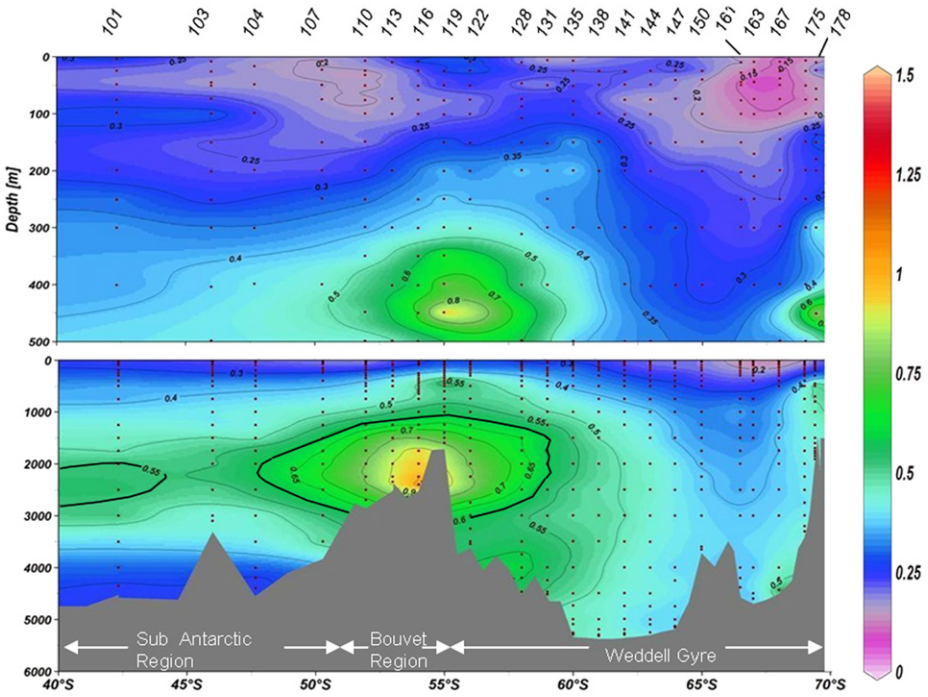

Fig. 5. Color and contour plot of the concentration of dissolved Fe (nM) of the transect in the upper 500 m (upper graph) at expanded vertical depth scale, and over the complete ~5000 m depth (lower graph). Dots indicate Fe datapoints, trace metal station numbers are indicated. This figure is made using Ocean Data View (Schlitzer, 2009).

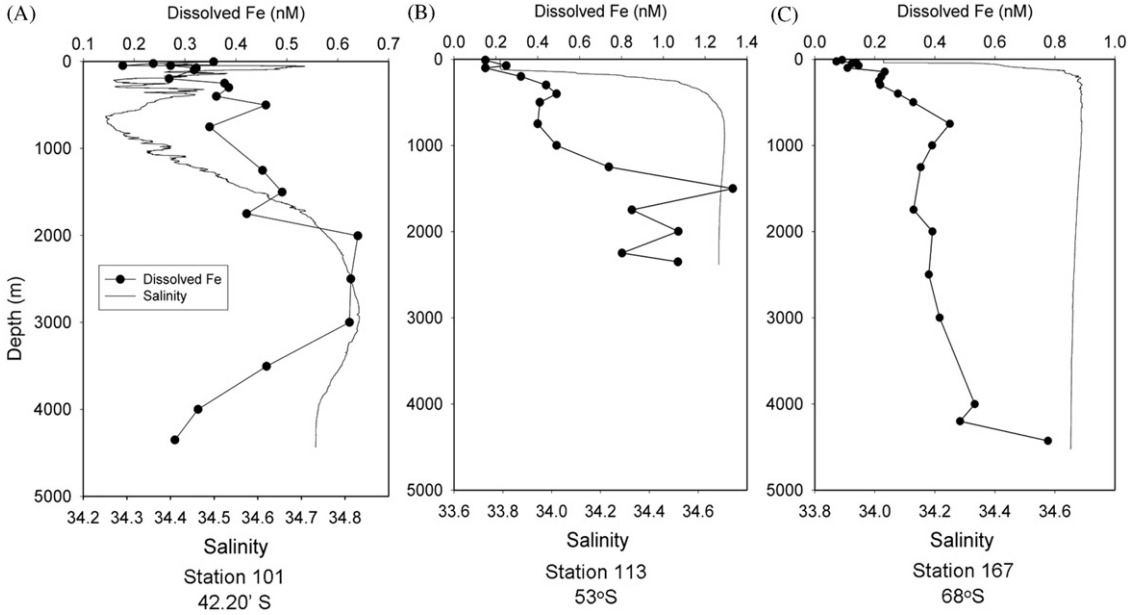

Fig. 6. Depth profiles of dissolved Fe (filled dots) and salinity (thin line) of station 101 (A), station 113 (B) and station 167 (C) as indicative of three distinct regions (see text).

3.3.2. Underway sampling of the southernmost surface waters

With the towed torpedo samples were taken from the very upper water column (2–3 m depth), thus represent the upper surface waters. Fig. 7 shows the concentrations obtained with the torpedo together with the averaged surface mixed layer concentration of dissolved Fe. From 66°S to 67°S (0.1–0.2 nM) dissolved Fe in the upper meters tended to be lower than the averaged surface mixed layer concentration. From 67°S southwards the concentration in the upper meters nicely followed the surface mixed layer average, with exception of concentrations at 67°16.34′S (~0.3 nM) and 67°45.57′S until 68°30.52′S (~0.3 nM). Very high (~0.7 nM) concentrations were observed at 66°33.82′S and 68°00.00′S. At the 66°33.82′S position this coincides with a strong salinity minimum (Fig. 7A) and the local observation of many icebergs. From 69°S southwards towards the continental ice-sheet, both the Fe in the upper 2–3 m and its averaged surface mixed layer concentration increased. The salinity at a 5 m depth was relatively constant at a value of around 34.2, till ~66°20′S (Fig. 7A). From there, the salinity values fluctuated from 34.03 to 34.13 with an exceptional depression to 33.93 at ~66°30′S. A strong increase was observed ($S=34.2$)

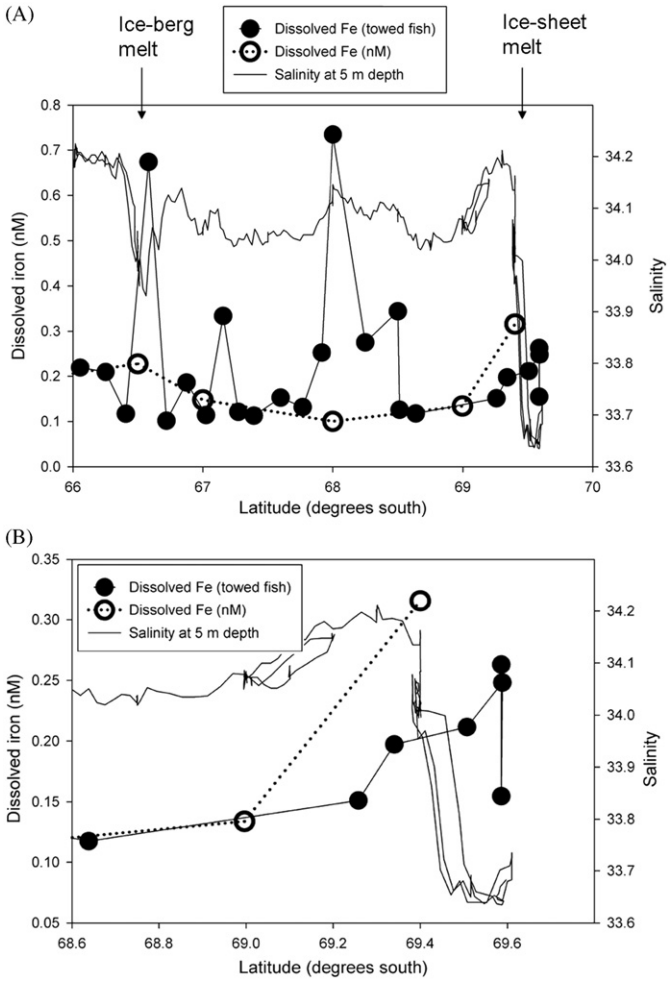

Fig. 7. (A) Transect plot of the concentration of dissolved Fe in the upper 1–2 m of the water column, as obtained by the towed fish (see text) (filled circles). Also plotted are surface mixed layer average Fe concentration collected with GO-FLO samplers (open circles) and the salinity at 5 m depth from the ships inlet (Fielax) (solid line with dots). Despite some mismatch in sampling inlets and their sampling depth as well, and patchiness of filaments of mixing (melt)waters, distinct Fe maxima tend to coincide with salinity minima due to meltwater. Observed melting of icebergs and the ice-sheet is indicated. (B) Same as (A), but at expanded scales (region adjacent to the ice-sheet). Notice increasing dissolved Fe coinciding with decreasing salinity due to meltwater. The three Fe samples at 69.36′°S were collected when the ship travelled straight westward in an open polynia, the different Fe values (0.26, 0.25 and 0.15 nM) illustrative of patchiness of meltwater.

at 69°00′S, followed by a decline of salinity towards the ice-sheet; the southernmost station at ~69°36′S had a salinity of 33.7. This is immediately adjacent to the massive ice-sheet extending from the continent, and many icebergs were also present.

3.4. Fe in the deep waters

Here, we follow the subdivision in three distinct regions (Fig. 6).

3.4.1. Subantarctic region

The properties of these waters are largely influenced by the intrusion at the 2000–3000 m depth of the North Atlantic Deep Water (NADW) (Gladyshev et al., 2008). The core of the NADW was located at the ~3000 m depth at station 101 (42°20′S) (Fig. 6A) and gradually rising to 2000 m depth at station 104 (47°40′S), although at the latter latitude the Fe rich NADW has been diluted strongly by mixing and was less pronounced (Fig. 5). The concentration of dissolved Fe was slightly elevated from 2000 to 3000 (~0.6 nM), compared to the overlying and underlying waters (~0.4 nM) (Figs. 5 and 6A).

3.4.2. Bouvet region

The deep waters above the ridge contained high concentrations of dissolved Fe compared to the waters South and North of the ridge. This high concentration was most prominent in the deeper waters and separated by a subsurface Fe minimum (0.05–0.20 nM) from the surface waters.

At stations 110 and 113 (52–53°S), the concentration steadily increased with depth from ~0.3–0.4 to ~0.55 nM at the 1250 m depth. This general increase in dissolved Fe with increasing depth coincided with the layer of relatively high salinity and potential temperature, which indicates mixing of LCDW with the NADW (Veth et al., 1997). At station 119 (~55°S), a maximum in dissolved Fe concentration of 1.2–1.8 nM was followed by decrease to ~0.8 nM Fe at the 1250 m depth.

The concentration of Fe in the LCDW varied with latitude; concentrations were about ~0.5 nM, interrupted by elevated concentrations (maximum 2.2 nM).

3.4.3. Deep Weddell Gyre

Also in the Weddell Gyre a subsurface minimum is observed. Below this minimum the concentration gradually increased until a relatively constant concentration of ~0.45 nM was observed at 750–1000 m (Figs. 5 and 6C). Below the AASW the Fe concentrations gradually increased with depth. The downward increase was less pronounced and was observed only at shallower depths in the Northern part of the Weddell Gyre (stations 128–141; ~57–62°S), compared to the Southern part (stations 141–175: ~62–69°S). At station 163 (~67°S) relatively low concentrations of ~0.4 nM Fe were found as deep as 2500 m, and these concentrations did not change towards the bottom (Fig. 6C). This region of relatively low (<0.4 nM) Fe concentration appears to coincide with a slight increase in salinity and potential temperature, which indicates the presence of WDW. Moreover, in the centre of the Weddell Gyre, out of the influence of the Bouvet Region, from stations 131 to 175 (59–69°S), dissolved Fe showed a negative relationship with potential temperature for waters with $\theta > -0.7$ °C and salinity >34.6 (comprising WDW and WSDW according to (Klatt et al., 2005)), as follows:

$$[\mathrm{Fe}] = -0.13\theta + 0.40 \quad (R^2 = 0.45, P < 0.01, n = 145) \tag{1}$$

as shown in Fig. 8 and discussed in Section 4.2.1.3.

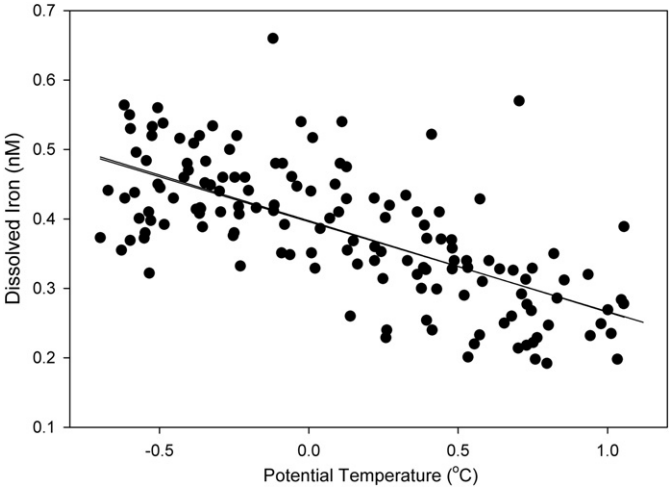

Fig. 8. Relation between dissolved Fe (nM) and potential temperature (θ) (°C) within the Weddell Basin, for all waters with $\theta > -0.7$ and salinity >34.6. (Deep waters: WDW, WSDW). $[\mathrm{Fe}] = -0.13\theta + 0.40$. ($R^2 = 0.45$, $P < 0.01$, $n = 145$.)

4. Discussion

4.1. The Fe cycle in the surface waters

4.1.1. Sources of dissolved Fe in the surface waters

The sources of the dissolved Fe in surface waters may be (i) from below by upwelling and vertical mixing of deeper Fe-rich waters, (ii) from above by partial dissolution of aerosol deposition, (iii) from seasonal melting of the seasonal sea-ice cover of the Southern Ocean, or from partial dissolution of sediment carried along from (iv) the Antarctic ice-sheet with calving and melting icebergs or (v) from the (Antarctic) continental margin sediments.

4.1.1.1. Upwelling and vertical mixing of deep waters with higher Fe concentration. Fe can be delivered in the surface waters from below, by both advective transport and turbulent diffusive fluxes (eddy-diffusion) (De Baar et al., 1995; Löscher et al., 1997; Croot et al., 2004). Here, we estimated the contribution of both processes, by using the same approach as De Baar et al. (1995) for all stations. For each station, we take the average value of all datapoints deeper than 1000 m as an estimate of the deep water concentration. The average value for all stations is 0.55 ± 0.19 nm ($n=222$). By multiplying with a typical annual average upwelling velocity of about 15×10^{-5} cm s^{-1} (Gordon et al., 1977), we obtain a typical annual average advective Fe flux of the order of 0.82 pmol m^{-2} s^{-1}. Due to the now established lower deep Fe concentrations than previously reported (Löscher et al., 1997) this advective upwelling transport is about half the advective flux (1.7 pmol m^{-2} s^{-1}) previously reported by De Baar et al. (1995) and Löscher et al. (1997), yet higher than the advective upwelling transport of 0.41 pmol m^{-2} s^{-1} reported by Croot et al. (2004). Large regional differences appear in the average annual advective fluxes; our average value within the ACC is 1.05 pmol m^{-2} s^{-1}, compared to 0.66 pmol m^{-2} s^{-1} in the Weddell Gyre. Moreover, seasonality in upwelling velocity is well known to occur but cannot be taken into account due to lack of seasonal observations thus far. Although the advective upwelling flux here is calculated per station, some uncertainties may arise by using the average Fe concentration > 1000 m There are some variations in deep Fe concentrations (Fig. 2). The standard deviation of all deep water concentrations, being 0.19 nM or 30% affects the derived annual average upwelling flux accordingly.

We also calculated the vertical mixing or eddy-diffusive flux defined as the product of the typical annual average vertical turbulent diffusivity coefficient (Kz) (3.0×10^{-5} m^{-2} s^{-1}) and δ[Fe]/δz (De Baar et al., 1995; Löscher et al., 1997). Here, δ[Fe]/δz is defined as the concentration difference in dissolved iron between the deepest value within the surface mixed layer and the shallowest value directly below the surface mixed layer. However, the differences in vertical distance to the base of the surface mixed layer varies between the different stations, introducing some small errors to the eddy-diffusive flux calculation. At 62–65°S a Fe minimum is observed directly below the surface mixed layer, at the depth of the fluorescence maximum. In these stations the dissolved iron concentration directly below the pycnocline is used as the deepest concentration, here taking pycnocline depth values after Middag et al. (2011a, Fig. 8). Due to a slight elevation of dissolved iron concentration within the very shallow surface mixed layer a negative (downward) eddy-diffusive flux is calculated at one station (station 150, ~65°S). Nevertheless, the annual average upward eddy-diffusive flux equals 0.034 pmol m^{-2} s^{-1} for the complete transect, which is comparable to the estimation of 0.048 pmol m^{-2} s^{-1} by Croot et al. (2004). On an annual basis, our reported total upward transport equals 27.07 μmol m^{-2} y^{-1} (26.01 plus 1.06 μmol m^{-2} y^{-1}) representing the average of a somewhat higher upward transport of 34.0 μmol m^{-2} y^{-1} in the ACC and a somewhat lower upward transport of 31.6 μmol m^{-2} y^{-1} in the Weddell Gyre. Measures and Vink (2001) reported 30–33 μmol m^{-2} y^{-1} transported by upwelling, and 0.47 μmol m^{-2} y^{-1} by vertical mixing in the Pacific sector of the Antarctic Circumpolar Current at 170°W, similar to our estimates. For the Australian sector of the Southern Ocean, at 140°W Sedwick et al. (2008) reported a vertical resupply of ~0.01 to 0.1 nM over a 4 month summer period due to eddy-diffusion. Our upward transport of 34.0 μmol m^{-2} y^{-1} in the ACC (SML depth ~100 m) and that of 31.6 μmol m^{-2} y^{-1} in the Weddell Basin (SML depth ~50 m) leads to an estimate of ~0.11 to 0.14 nM increase for the same period, and thus 0.33–0.42 nM/y. Overall the rates of advective upwelling transport are virtually the same in the Pacific and Atlantic sectors, but the Fe supply rate of vertical mixing appears to be larger in the Atlantic part of the Southern Ocean (this study; Croot et al., 2004). In the Australian sector of the Southern Ocean, Lai et al. (2008) also ascribed higher Fe concentrations in surface waters to upwelling deep waters, as confirmed by high salinity, temperature and silicate concentrations.

4.1.1.2. Fe sources from atmospheric deposition. Input of dissolved Fe by dissolution of aeolian transported particles (dust) originating from land is a well recognized mechanism (Martin and Fitzwater, 1988; Fung et al., 2000; Jickells et al., 2005; Cassar et al., 2007; Planquette et al., 2007). Dissolved Al is deemed a suitable tracer for dust deposition (Measures et al., 2008; Han et al., 2008). We here calculated dissolved Fe and Al averaged over the upper 25 m from the vertical sampling (Fig. 9, Table 1). Surface Al and Fe show a weak similarity along the transect (Fig. 9). When we exclude station 178, nearest to the ice-sheet (where surface water Fe is influenced by ice melt, Section 4.1.1.4), we observe a weak but significant correlation between the upper 25 m averaged dissolved Fe and Al, as follows:

$$[\mathrm{Fe}] = 0.15[\mathrm{Al}] + 0.12 \quad (R^2 = 0.46, P < 0.01, n = 21) \qquad (2)$$

The here observed Fe:Al ratio of 0.15 is lower than the ratio 0.26 for the continental crust reported by Wedepohl (1995), but is not very different from the ratio of 0.19 reported by Mackie et al. (2006) for precipitated dust. Removal of dissolved Fe due to uptake by phytoplankton can lower the Fe concentration compared to Al, leading to a slightly lower Fe:Al ratio. Although estimations of the share of wet deposition to the total worldwide deposition vary from 23% to 73% (Jickells and Spokes, 2001), the importance of wet

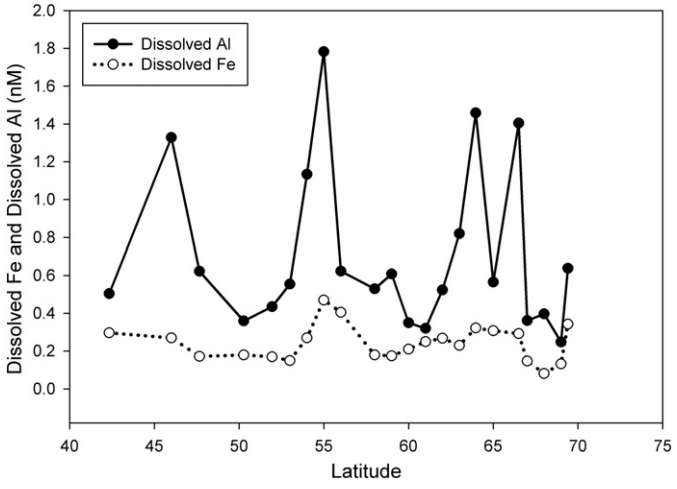

Fig. 9. Transect plot of concentrations of dissolved Fe (open circles) and dissolved Al (filled circles) in the upper 25 m of the water column. For deriving a correlation between Al and Fe, the southernmost station near the ice-sheet has been excluded (Eq. (2), see Section 4.1.1.3).

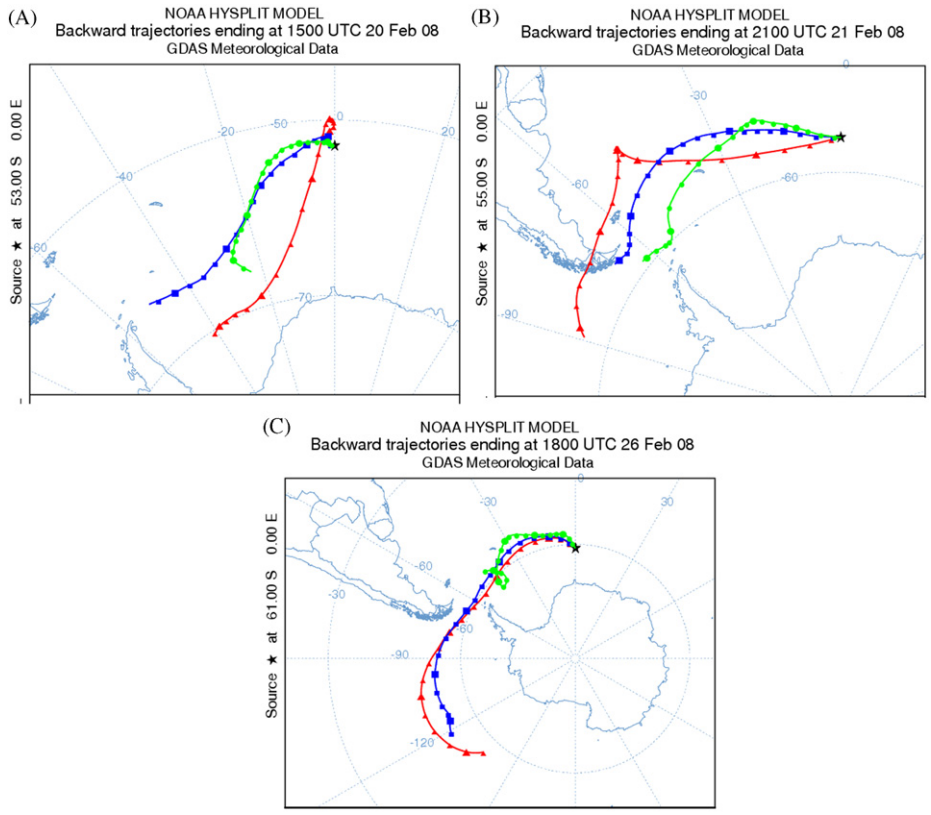

Fig. 10. Five day (120 h) back-trajectory analyses for air parcels at elevations of 10 (green), 500 (blue) and 1000 (red) m, as calculated using the NOAA HYSPLIT model (Draxler and Rolph, 2003). The back-trajectories start from (A) 53°00.00S at 15:00 UTC on February 20, 2008, (B) 55°00.00 S at 21:00 UTC on February 21, 2008 and (C) 61°00.00 S at 16:00 UTC on February 26, 2008, respectively.

deposition is confirmed by Hand et al. (1999) and Wolff et al, 1998 (summarized by Hand et al., 1999). During the transect we encountered a strong rain event with 0.3 mm h^{-1} on average at 53°48′S and another rain event with an average of 0.18 mm h^{-1} at 55°40′S (data not shown). Therefore the local elevated concentrations of dissolved Fe and Al observed in the upper 25 m (Fig. 9) around 54–56°S are ascribed to recent wet deposition. This is consistent with previous findings of Croot et al. (2004) in the region. Air mass back-trajectories (Fig. 10A) are consistent with dust input originating from Patagonia causing elevated dissolved Fe and Al at about 55°S (Fig. 10B), in contrast to the adjacent regions (Fig. 10A and C).

Dust deposition model studies show a gradual decrease in dust deposition towards the south (Mahowald et al., 1999; Duce and Tindale, 1991; Cassar et al., 2007) and recognize the relatively high contributions of dust coming from Patagonia, reaching almost as far east as the zero meridian at ~55°S. Using such model results, the transect here occupied lies completely within the 0–0.2 g m^{-2} y^{-1} deposition range (Jickells et al., 2005; Mahowald et al., 2005). According to Duce and Tindale (1991) the dust deposition range over the transect varies from >0.1 g m^{-2} y^{-1} in the north part of our transect to <0.01 g m^{-2} y^{-1} towards the Antarctic continent. Recently, an increase in solubility with decreasing dust concentrations was reported (Baker and Croot, 2008). Baker et al. (2006) report a median value of 8.3% solubility in the remote South Atlantic and Edwards and Sedwick (2001) reported a median value of 32% solubility in samples of snow from Antarctica. Hence, we take the 8.3% solubility for the remote South Atlantic (and 0.1 g m^{-2} y^{-1} dust deposition (Duce and Tindale, 1991) as a lower limit and the 32% solubility of Antarctic snow (and 0.01 g m^{-2} y^{-1} dust deposition (Duce and Tindale, 1991) as an upper limit. Using a Fe content of dust of ~3.5%, as reported by Taylor and McLennan (1985) and used by Mahowald et al. (2005), this results in an influx rate of Fe dissolved from dust between 2 and 5.2 × 10^{-6} mol m^{-2} y^{-1}. In terms of the concentration of dissolved Fe over an average 65 m deep SML, this would represent an annual increase of 0.03–0.08 nM due to dust input alone. This is an order of magnitude lower than the atmospheric Fe influx reported by Sedwick et al. (2008) north of the Polar Front, in the Australian Sector of the Southern Ocean. This difference may partly be explained by differences in the dust deposition; Jickells et al. (2005) and Mahowald et al. (1999) estimated the dust deposition directly South of Australia to be between 0.2 and 2.0 g m^{-2} y^{-1}, roughly an order of magnitude higher than the flux over the zero meridian. Lancelot et al. (2009) suggest a modeled dust deposited Fe flux of 0.02–0.1 pmol m^{-2} s^{-1} over the zero meridian, which is in close agreement with our findings.

4.1.1.3. Melting of seasonal sea-ice. Several studies discuss the seasonal melting of sea-ice as a possible mechanism of dissolved Fe input in the Surface Mixed Layer (SML) (Löscher et al., 1997; Measures and Vink, 2001; Croot et al., 2004; Lannuzel et al., 2008). Simulations of the Antarctic sea-ice extent by the University of Bremen (http://iup.physik.uni-bremen.de:8084/amsr/amsre.html) show that our study region is virtually sea-ice free throughout February 2008 till the end of March 2008. The freshwater released by sea-ice melt earlier in the season causes a relatively fresh layer on top of the more saline, colder winter water (WW) (Park et al., 1998, Fig. 4). From 60°S to 69.24′°S (stations 135–178), we can clearly distinguish the latter more saline colder winter water (WW) with potential temperature of ~ -1.65 °C and salinity of ~34.34,

using data from the CTD profiles in our stations. If we assume that the salinity deficit between the surface and the winter water is caused *solely* by sea ice melt, and sea-ice salinity is 5 (ice plus brine; Eicken, 1992) we can calculate the apparent winter sea-ice thickness by integrating the salinity deficit at each depth from surface to winter water. This is a similar approach as used by Hoppema et al. (2007) with regard to nutrient depletion. Using this approach we find the reconstructed apparent winter sea-ice thicknesses in the range 33–163 cm, with an average of 58 ± 30 cm ($n=11$). There is a clear distinction between the stations 135 and 167 from 60°S to 68°S with an average of 47 ± 13 cm ($n=9$) and the final two stations 175 and 178 near the ice-sheet (69°S and 69°24′S), with the highest estimates of 67 and 163 cm, respectively. Worby et al. (2008) find, in the period with maximum sea-ice extent (spring; September–October–November) an average sea ice thickness of 89 cm and an ice coverage of 82% in the East Weddell Gyre (45°W–20°E). This would correspond to an overall 73 cm thickness for a presumed 100% coverage.

Lannuzel et al. (2008) studied temporal changes in dissolved Fe concentration of Weddell Sea pack ice. They found vertical integrated dissolved Fe concentrations of 1.1–13.3 μmol m^{-2} and total dissolvable (dissolved plus particulate) concentrations of 6.1–59.4 μmol m^{-2} in the ISPOL station in the Weddell Sea. This vertical integrated value comprises brine, sea-ice and snow for a 90 cm deep ice-core. For our reconstructed average sea ice thickness of 58 ± 30 cm this would correspond to a range with the lower value of 0.34 μmol m^{-2} (the dissolved Fe in the sea-ice) and a higher value of 57.5 μmol m^{-2} as upper limit in the case that all the particulate Fe in the sea-ice would also dissolve. Over a ~40 m SML (average 60–69.24′°S) this equals a 0.01–1.43 nM Fe supply from ice melt. Nevertheless, the here used sea-ice thickness and Fe concentrations vary widely between different regions (Lannuzel et al., 2008), which results in major uncertainties in the Fe flux from the sea-ice to the ocean, beyond our estimated range. It should be noted that seasonal sea-ice can be seen as a storage of Fe captured from the surface waters during autumn sea-ice formation and external Fe supply of dust deposition accumulated in snow on top of the sea-ice (Lannuzel et al., 2008). During melting season this Fe will be released in a relatively short period of time leading to temporarily increased Fe supply.

4.1.1.4. Fe sources from the Antarctic continental ice-sheet and free drifting icebergs. The melting of the Antarctic ice-sheet or that of free-ranging icebergs are alternative input sources of dissolved Fe to the surface waters (Croot et al., 2004). This Fe originates either from dust blown from Patagonia, or from contact of the ice-sheet with the underlying continent or from grounding of icebergs over the shelf. Obviously these processes result in a very heterogeneous distribution of Fe in the ice, as indeed shown in the very wide natural range of Fe concentrations between 0.52 and 120 nM in land-ice (Edwards et al., 1998) or 10.8 and 99.3 nM (Löscher et al., 1997) in meltwater from icebergs. In two regions (~69°24′S and ~66°30′S) higher dissolved iron coincides with extreme salinity minima (Fig. 7A). In Section 4.1.1.3 all salinity minima in the surface water had been ascribed *solely* to melting of seasonal sea-ice. Here alternatively, we assess implications when one would ascribe the two extreme salinity minima *solely* to the melting of the continental ice-sheet and/or free drifting icebergs. When comparing the background salinity 34.084 along 66–69°S with the minimum 33.653 at 66°36′S we derive a local 1.3% ice-sheet meltwater contribution. Now taking [Fe] of 0.15 nM of 69°15′S as background value and the highest 0.26 nM as enhanced due to this 1.3% ice-sheet meltwater one may derive

$$\begin{aligned} Fe_{mixture} &= 0.26\,nM = (0.987\,Fe_{Seawater}) + (0.013\,Fe_{ice\text{-}sheet}) \\ &= (0.15\,nM) + (0.11\,nM) \end{aligned} \quad (3)$$

from which we derive an apparent Fe concentration in the ice-sheet end-member of 8.6 nM. Similarly, in the salinity minimum region at ~66°30′S, where a high abundance of icebergs was observed, one may derive 0.86% ice berg meltwater, hence the observed Fe concentration difference of 0.56 nM would be consistent with a Fe content of 66.4 nM in the iceberg end-member. The apparent ice-sheet end-member of 8.6 nM and apparent ice-berg end-member of 66.4 nM fall within the above mentioned wide and variable natural range previously reported. Thus the melting of ice-sheet or icebergs may, in principle, account for the Fe maxima coinciding with the extreme salinity minima, but likely several other processes, such as sea-ice melting or biological interactions also play a role. Finally due to the very wide natural variability of Fe content of ice-sheet and icebergs, in combination with the major uncertainty in the percentage of total Fe that will dissolve in meltwater or seawater, we reckon that an accurate assessment of Fe supply by ice-sheet and icebergs will always remain very difficult. At best one may realize that these may, or may not, be significant sources of dissolved Fe to the surface waters of the Southern Ocean.

4.1.1.5. Continental ice-sheet of Antarctica prevents Fe supply to surface waters from continental shelf sediments. The continental shelves surrounding the islands in the Southern Ocean, such as Bouvet, Kerguelen and Crozet are known to bring significant elevated Fe concentrations to the deep oceans (Croot et al., 2004; Planquette et al., 2007; Blain et al., 2007, 2008a, 2008b). In addition, Sohrin et al. (2000) reported patches of elevated iron south of the Polar Front at 140°E, which was (partly) attributed to organic rich sediments from the slope.

During ANT XXIV/3 however, no indication of significant input from organic rich sediments from the continental shelf of the Antarctic continent was observed. This is likely due to the extension of the continental ice-sheet quite far into the ocean basin. Our southernmost station (178) at 69°24.03′S was located very close to the 200 m thick ice-sheet, but was still > 2000 m deep. The common occurrence of plankton blooms in this region directly adjacent to the ice-sheet may well yield significant export of organic carbon to the underlying slope sediments, and upon its oxidative bacterial degradation in the surface sediments the ensuing suboxic conditions may well yield reductive dissolution of Fe (see Section 4.2.1.3, Elrod et al., 2004). However such reducing sediments here are far too deep (> 2000 m) for any significant input into the local surface waters. Below the extended ice-sheet itself (Middag et al., 2011a, Fig. 13) there is deemed to be no biological production, thus the only and presumably very insignificant export of organic matter to the seafloor is by lateral input from biological production in waters outside the ice-sheet extent. Rutgers van der Loeff et al. (2011) reported a C export flux of 9.9 mmol C m^{-2} d^{-1} at 100 m depth at the station (178) nearest to the ice-edge. However, they mention that this is most likely an overestimation due to advective fluxes. The C export at stations further in the basin was low; 3.1–4.5 mmol C m^{-2} d^{-1} (Rutgers van der Loeff et al., 2011). Hence the seafloor of the continental shelf under the extended ice-sheet likely comprises very low organic carbon. Such low organic supply is unlikely to lead to suboxic let alone anoxic conditions. Therefore, these local sediments are unlikely to be a reductive source for dissolved Fe (or Mn) to the overlying bottom waters and in turn to the surface waters. In contrast to continental shelf sediments throughout the world, the unique permanent ice-sheet extending off the Antarctic continent at the zero meridian largely prevents the normal biogeochemical mechanisms for mobilization of Fe and Mn (Middag et al., 2011a) from the underlying shelf sediments. Thus Antarctica is unique because when approaching from the open ocean the dissolved Fe and Mn tend to decrease, as opposed to the always increasing trend towards all other continents (De Baar and De Jong, 2001).

The Fe measured in acidified unfiltered samples during the ANT XXIV/3 cruise provides information about the labile fraction of the particulate Fe. However, no unfiltered samples were collected at stations near the ice-sheet, precluding additional information.

4.1.2. Removal of Fe from surface waters

Dissolved Fe predominantly exists in the trivalent Fe(III) oxidation state in seawater, of which the large majority is bound by organic Fe-complexing moieties (Thuroczy et al., 2011). In general the Fe(III) state is very "particle-reactive" and tends to adsorb to small colloids within larger (>0.2 μm) size classes, causing a sinking loss term of Fe from surface waters. Moreover, Fe is taken up directly by phytoplankton and bacteria (De Baar and De La Roche, 2003), and upon predation of these by micro- and mesozooplankton and krill, part of the intracellular Fe may become dissolved again (Sarthou et al., 2008). Yet another part may end up in large fecal pellets that tend to settle down into deeper waters (Tovar-Sanchez et al., 2007; Hutchins and Bruland, 1994).

Below, an effort is made to distinguish between (i) the biological uptake inside the living plankton cell, and (ii) scavenging and sinking loss.

4.1.2.1. Fe removal by biological uptake. Uptake by phytoplankton and subsequent export from the surface mixed layer is an important mechanism for iron removal from the mixed layer (Coale et al., 2005). Mixed layer average concentrations of dissolved Fe and chlorophyll fluorescence (Table 1) are shown in Fig. 11. North of the Polar Front (41–46°S) southward decreasing Fe (~0.3 to ~0.2 nM) coincides with relatively high fluorescence. South of the Polar Front within the AAZ (50–55°S), a weak but significant negative correlation was found:

$$\text{Fluorescence} = -0.67\,\text{Fe} + 0.37 \quad (R^2 = 0.39, P < 0.01, n = 19) \qquad (4)$$

Further southwards in the Weddell Gyre (56–69.24′S) a similar trend was found:

$$\text{Fluorescence} = -3.99\,\text{Fe} + 1.45 \quad (R^2 = 0.41, P < 0.01, n = 25) \qquad (5)$$

The southernmost station (178) at 69°24′S, is strongly influenced by the Antarctic ice-sheet, hence is excluded from the relationship in (Eq. (5)). The slope of the relationship (Eq. (5)) between dissolved Fe and fluorescence within the Weddell Gyre is significantly steeper than the preceding relationship (Eq. (4)) within the AAZ ($P < 0.05$, 2-sided t-test).

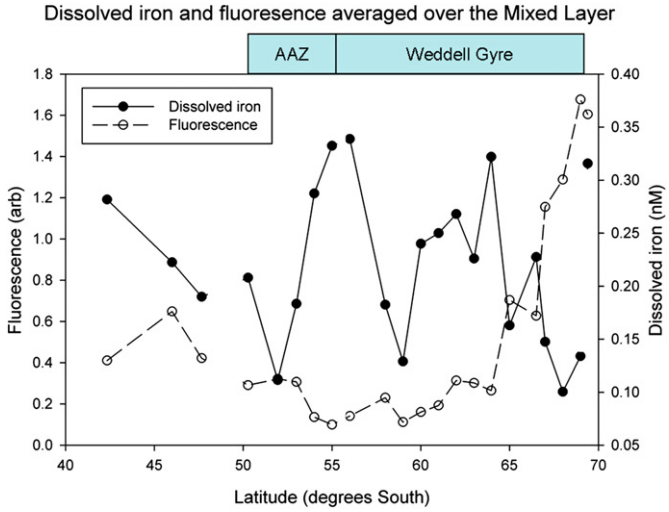

Fig. 11. Transect plot of the average concentration (nM) of dissolved Fe (filled circles) and fluorescence (open circles) in the upper Surface Mixed Layer (SML). Each datapoint is the average of 2–4 independent datapoints for shallow and deep SML, respectively. The five datapoints for the AAZ (50–55°S; stations 107, 110, 113, 116 and 119) represent 19 independent datapoints as used for Eq. (4) (Section 4.2.1.2); the 13 datapoints for the Weddell Gyre (56°S–69.24′S, stations 122–175) represent 25 independent datapoints as used for Eq. (5).

While realizing that other factors also affect the Fe concentration in the surface water, the significant negative relations (Eqs. (4) and (5)) between fluorescence and dissolved Fe here suggest that removal of dissolved Fe by phytoplankton primary production has occurred in the time preceding our study. This is supported by findings of Middag et al. (2011a), who also report uptake of the biological essential trace metal Mn by phytoplankton in the SML along the same transect.

We can calculate the removal of Fe from the upper waters over the complete transect until the ice-edge (Section 4.1.1.5). Using the average carbon export (5.3 ± 2.4 mmol C m^{-2} d^{-1}; Rutgers van der Loeff et al., 2011) and a C:Fe ratio of $\sim 10^5$ (Twining et al., 2004), we obtain an estimation of the Fe removal of $0.06 \pm 0.03 \times 10^{-6}$ mol m^{-2} over the preceding four months (summer). Using a typical sinking velocity of 40 m d^{-1} (Garrity et al., 2005) leads to a seasonal export of 0.16 ± 0.07 nM. However, it should be noted that our cruise took place in late austral summer, conceivably leading to a relative high estimation of the carbon export, perhaps resulting in an overestimation of the biological drawdown. Nevertheless, in another region, at about 140°E south of the PF, and with another approach based on spring Fe data and seasonal nitrate drawdown, Sedwick et al. (2008) calculated a very similar value of seasonal biological drawdown of Fe of ~0.14–0.18 nM. A Fe drawdown of the same magnitude (~0.24 nM) was derived by Measures et al. (2001) at 170°W. Chlorophyll a can be ascribed largely to diatoms, as they are a very important phytoplankton group within the Southern Ocean, where diatoms tend to dominate under high silicate conditions (Sarthou et al., 2005). At our transect, in the northernmost (stations 101–107), haptophytes and chlorophytes dominated the phytoplankton community. All other stations from station 107 to the ice-sheet had a diatoms dominated community (except at station 141, ~62°S). (Alderkamp et al., 2010; Neven et al., 2011).

4.1.2.2. Fe removal by adsorptive scavenging. In addition to true biological uptake, adsorptive scavenging on settling particles (both biogenic and lithogenic) is a mechanism of Fe removal from the upper ocean (Wu et al., 2001). However, dissolved Fe is strongly protected from scavenging by binding to dissolved organic ligands (Wu et al., 2001; De Baar and de Jong, 2001) and for this transect assessed by Thuróczy et al. (2011).

4.2. The Fe cycle in deep waters

4.2.1. Sources of Fe to deep waters

The distribution of dissolved Fe in the deep waters of this part of the Southern Ocean is largely influenced by (i) the inflow of different water masses, (ii) the input by hydrothermal vents and (iii) the input from reductive sediments.

4.2.1.1. Inflow of NADW rich in dissolved Fe. The vertical profiles of salinity and nutrients make clear that the deep waters in the North East part of the transect were largely influenced by NADW. Higher dust input at the surface (Moore and Braucher, 2008), a closer proximity to the continent and mixing of water masses with enriched iron (Labrador Sea, Mediterranean Sea) (Laës et al., 2003) cause elevated concentrations of Fe in the NADW in the Atlantic Basin. The intrusion of NADW into the Southern Ocean is clearly marked by higher Fe and lower NO_3 concentrations progressing southwards at 2000–3000 m depth (Figs. 3, 4A, 5, 6A). This NADW affects the Fe concentration in the circumpolar waters north of the Bouvet region. The concentrations found in the NADW (~0.6 nM) are consistent

with the lower range of the values of 0.6–1.0 nM reported previously by Löscher et al. (1997) for a station at 50°S, 6°W. Based on the northernmost profile (Fig. 6A) we make an estimation of the net input of NADW (~0.61 nM) to the Southern Ocean (~0.41 nM) by the difference of ~0.2 nM. We can multiply this concentration difference with the total volume transport of 930×10^{12} m^{-3} y^{-1} of NADW into the Atlantic Sector (20°E to 65°W) of the Southern Ocean (De Baar et al., 1997) and dividing by the total surface area of 2.05×10^{13} m^2 of latter Atlantic sector (Losch, AWI, personal communication) would yield in an influx of 9.1×10^{-6} m^{-2} y^{-1}.

4.2.1.2. Hydrothermal vent input at the ridge crest in the Bouvet region. At the Bouvet region, hydrothermal activity is deemed to be the cause of the above mentioned (Section 3.4.2) elevated Fe and Mn concentrations within the shown contour (Fig. 5). For a similar, but stronger hydrothermal anomaly in the Arctic Ocean, this was accompanied by significant anomalies of temperature and suspended particles (lower light transmission), as well as anomalies in calculated [Al/(Al+Mn+Fe)] × 100 ratio values (Klunder et al, in preparation). Briefly, Boström and Peterson (1969) have shown that hydrothermal (metalliferous) sediments are enriched in Fe and Mn and relatively depleted in lithogenous elements such as Al, and were able to demonstrate this hydrothermal component with the [Al/(Al+Mn+Fe)] × 100 ratio concept. Here over the Bouvet region a temperature anomaly was not discernible, but lower light transmission was found from 1600 depth to the seafloor at ~53°31′S (not shown) and accompanied by anomalous element ratio values indicative of hydrothermal Fe input (Fig. 12).

4.2.1.3. Input into subsurface waters from sediment sources elsewhere. Within the upper 500 m of the water column (Fig. 5, upper graph) two distinct subsurface maxima were found, just south of the Bouvet region and adjacent to the Antarctic continent, respectively.

At the stations over (station 119) or just south (stations 122 and 128) of the ridge a maximum of dissolved Fe was observed at intermediate depth range (Fig. 5; 400–700 m depth). At station 128 this is confirmed by a maximum of labile particulate Fe at 500 m depth (Thuroćzy, 2009, personal communication). These Fe maxima might have originated from the shelf sediments of the Bouvet region. However, the maxima are located relatively high above the deep seafloor and there is a layer with lower dissolved Fe in between the maxima and the seafloor. Therefore, we suggest these Fe maxima to derive from the continental shelf of the Antarctic peninsula which is situated upstream of the ACC and the Weddell Gyre passing our zero meridian section. As shown in Fig. 1, the ocean topography along the flow path is relatively shallow, and geostrophic velocities are strong (Klatt et al., 2005), enabling Fe to be transported far from the peninsula towards the zero meridian. Moreover on the second transect crossing the Weddell Sea, and the third transect across Drake Passage, we indeed found elevated dissolved Fe over the shelf of the Antarctic peninsula (Klunder, in preparation). Moreover, Lam et al. (2006) showed that sediment transport from continental margins can indeed be a source of Fe over distances of 900 km.

At station 178, the high concentrations of > 1 nM at 450–500 m correspond with maxima of salinity and potential temperature (data not shown). Klatt et al. (2005) show that these are features of the westward flowing Antarctic Coastal Current. Therefore we state that these elevated Fe concentrations are to be explained by transport of Fe with the Antarctic Coastal Current. Here we also find an oxygen minimum and from 300 to 450 m depth, lower light transmission, i.e. higher abundance of suspended particles. Thus resuspension of particles from the more eastward shelves and subsequent dissolution could be a possible Fe source here. The sedimentary flux as suggested by Lancelot et al. (2009) in a modeling study is > 0.5 pmol m^{-2} s^{-1} close to the continent and < 0.02 pmol m^{-2} s^{-1} above the open ocean. Another model exercised by Tagliabue et al. (2009) suggests a stronger impact of sedimentary Fe input compared to that of dust Fe input. In both model simulation studies sedimentary Fe input is a function of bottom topography and neither the now observed Fe fluxes from hydrothermal input, nor the northerly water masses (NADW) brought to the surface by upwelling, nor the adverse effect of the ice-sheet on Fe fluxes, had been taken into consideration in preceding model simulation studies.

4.2.1.4. Fe supply into deep waters of the Weddell gyre. The dissolved Fe concentration varies between the different water masses within the Weddell Gyre. The water transport in the Weddell Gyre is well described by Klatt et al. (2005). The deep water masses (WDW, WSDW and WSBW) (see Section 3.1) are defined as waters with salinity > 34.6. Between ~56°S and 62°S (stations 122–141), where the Weddell Gyre flows eastward, the concentration of dissolved Fe in these deep waters is significantly ($P < 0.01$, 2-tailed homeoscedastic students t-test) higher (0.47 nM ± 0.16, $n = 98$) than the concentrations (0.33 ± 0.14, $n = 126$) in the westward

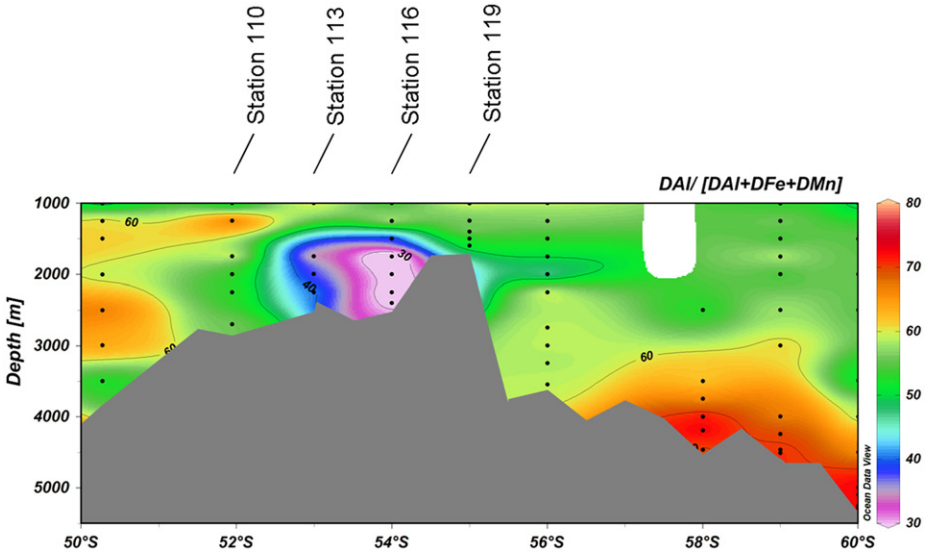

Fig. 12. Color plot of [DAl/(DAl+DFe+DMn)] × 100 ratio for the zero meridian transect; stations 110, 113, 116 and 119 are indicated (see also below 11b) This figure is made using Ocean Data View (Schlitzer, 2009).

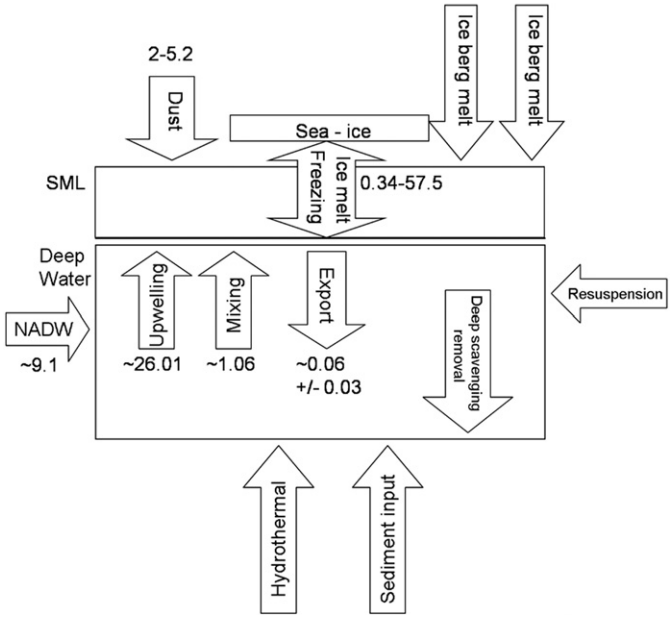

Fig. 13. Schematic of Fe fluxes towards an eventual Fe budget of the Atlantic Sector of the Southern Ocean. For several fluxes an estimate [10^{-6} mol m^{-2} y^{-1}] is given in the graph, see main text for derivation of estimates. For other fluxes a basinwide estimate in 10^{-6} mol m^{-2} y^{-1} units is not feasible. Melting of the continental ice-sheet would account for a local influx of 0.11 nM. Similarly at ~66°S, melting of free-drifting icebergs may account for a local increase of 0.56 nM. However, latter numbers are subject to large deviations and are therefore not in included in the graph. Moreover, there are strong indications of local Fe supply from hydrothermal activity, reducing sediments and sediment re-suspension,; see main text, but extrapolation to a basinwide estimate is as yet not feasible either.

flow, between ~62°S and 69°24′S (stations 144–178). From the relationship between potential temperature (θ) and dissolved Fe (Fig. 8) we conclude that the distribution of dissolved Fe is strongly dependent on ocean circulation and mixing. The Fe concentrations in the WDW ($\theta > 0$) are lower than in the WSDW ($-0.7 < \theta < 0$) (Klatt et al., 2005). Dissolved Fe, Mn and light transmission data suggest that the westward flow of the Weddell Gyre, coming from the remote Indian sector of the Southern Ocean, at high latitudes (stations 141–178; 62–69°24′S) contains slightly clearer water (higher light transmission values due to less particles) and lower trace metal concentrations, compared to the more northerly, eastward flowing waters of the Weddell Gyre (122–141; 56–69°S). The latter waters have been flowing along the North Weddell Ridge, where presumably there has been entrainment of particles coming from the slope sediments of the ridge. Also hydrothermal inputs from Bransfield Strait (Klinkhammer et al., 2001) may have contributed Fe to these eastward flowing waters. Another important input source for Fe in deep waters is reductive dissolution. Locally, some stations show slightly elevated (by ~0.2 nM) concentrations towards the bottom (178, 167 (Figs. 5 and 6C)).

4.2.2. Removal of dissolved Fe from deep waters

4.2.2.1. Upward advective upwelling supply and vertical mixing. The supply of Fe by upwelling and vertical mixing is extensively described in Section 4.1.1.1. Supply to the upper oceans implicates the removal of dissolved Fe from the deep waters by the water replacing the upper ocean waters, because the concentrations of dissolved iron in the upper waters are lower (~0.2 nM) than the concentrations in the deep (~0.4 nM) (Figs. 2, 5, 6). Thus we suggest a removal rate of 0.85 pmol m^{-2} s^{-1} (as calculated in Section 4.1.1.1) by hydrography of advective upwelling and vertical mixing.

4.2.2.2. Competition between stabilization by organic complexes and removal by scavenging onto settling particles. Dissolved Fe can be removed from the deep waters by scavenging onto sinking biogenic particles (see Section 4.1.2.2). Although lower than in the surface waters, also in the deep waters there still is an excess of organic ligands over dissolved Fe (Thuróczy et al., 2011), counteracting the adsorptive scavenging removal of dissolved Fe. However, ~42% of the dissolved Fe is within the "colloidal" fraction (here operationally defined as 1000 kDa $-$ < 0.2 μm) in the waters below 1000 m (Thuróczy, personal communication, 2009). Thus coagulation, aggregation and subsequent settling of these particles will remove a part of the dissolved iron from the deep waters. This mechanism is suggested also in the Pacific and Atlantic Oceans by Wu et al. (2001). Walter et al. (2000) also observed scavenging in the Weddell Sea, although in a relatively low quantity due to the low particle fluxes. Because this mechanism will create aggregates with sizes larger than 0.2 μm, an increase with depth may be conceivable for the "labile particulate Fe" in the water column (Thuróczy et al., 2011). Indeed, an increase with depth was observed from < 1 nM in the upper 1000 m to 2.77–8.31 nM for the deepest samples, at the five measured stations (103, 107, 128,131,163) along the zero meridian (Thuróczy et al., 2009 (personal communication).

Finally, Fig. 13 provides a schematic overview of the processes causing in- and output fluxes of Fe to the SML and deep waters as discussed above, and where possible an estimate [10^{-6} mol m^{-2} y^{-1}] of the flux is given in the graph. For some other fluxes we cannot yet give such a value.

5. Conclusions

The average dissolved Fe in the upper surface mixed layer of the Atlantic sector of the Southern Ocean varies between 0.1 and 0.3 nM. The most important source of dissolved Fe to the upper surface mixed layer is advective upwelling, which tends to be one order of magnitude higher than the upward Fe supply by vertical mixing. We conclude that the contribution of dust deposition as predicted using dust deposition models and our data is 5–10 times smaller than advective upwelling. Nevertheless, this study also shows that local and temporal input events as dust deposition and ice melt can cause considerable (presumably short term) elevations in the concentration of dissolved Fe. Supply by aeolian wet deposition events may be of local significance but cannot yet be accurately quantified in the context of a basinwide annual Fe budget of the overall surface waters. Iron uptake by phytoplankton and scavenging can decrease dissolved Fe concentrations in the upper layer.

In the deep waters, elevated Fe concentrations in the Subantarctic region are caused by intrusion of NADW to these SubAntarctic waters. The presence of elevated dissolved Fe over the ridge crest in the Bouvet region suggests a far more significant role than hitherto realized of hydrothermal vents as a major source term of Fe and Mn for deep waters of ocean basins. Furthermore, dissolved Fe in the eastward extent of the Weddell Gyre is significantly higher than in deep waters of the westward deep return flow. The slightly higher concentrations in the eastward flowing part of the Weddell Gyre are tentatively ascribed to hydrothermal iron inputs from Bransfield Strait and/or dissolution processes from the slope sediments of the North Weddell Ridge. The Antarctic continental ice-sheet extends well beyond its grounding line and therefore also covers the water column over the Antarctic shelf and slope. This largely prevents biological production, hence strongly minimizes the biogeochemical cycling over and within the shelf and slope. This subsequently minimizes lateral supply of Fe (and Mn) from the shelf and slope into adjacent open ocean waters. Thus in contrast to all other continental margins of the world, the dissolved Fe around Antarctica is lower towards the continent.

Acknowledgments

The authors are most grateful to the captain, officers and crew of FS POLARSTERN for their excellent support and commitment throughout the expedition ANT XXIV-3. This research was supported by NWO under project number XXXXX of the 2007-1008 International Polar Year Program. We would like to thank A. Bowie and two anonymous reviewers for their helpful and constructive comments. We also would like to thank Sven Ober from the Royal NIOZ and Gerd Rohardt from the Alfred Wegener Institute for providing the physical parameters. We commemorate our colleague Willem Polman who unfortunately did not return from ANT XXIV-3.

Appendix A. Supplementary material

Supplementary data associated with this article can be found in the online version at doi:10.1016/j.dsr2.2010.10.042.

References

Alderkamp, A.-C., De Baar, H.J.W., Visser, R.J.W., Arrigo, K.R., 2010. Can photoinhibition control phytoplankton abundance in deeply mixed water columns of the Southern Ocean? Limnology and Oceanography, 55(3), 1248–1264.

Aguilar-Islas, A.M., Resing, J.A., Bruland, K.W., 2006. Catalytically enhanced spectrophotometric determination of manganese in seawater by flow-injection analysis with a commercially available resin for on-line preconcentration. Limnology and Oceanography: Methods 4, 105–113.

Baker, A.R., Croot, P.L., 2008. Atmospheric and marine controls on aerosol iron solubility in seawater, Marine Chemistry. 10.1016/j.marchem.2008.09.003.

Baker, A.R., Jickells, T.D., Witt, M., Linge, K.L., 2006. Trends in the solubility of iron, aluminium, manganese and phosphorus in aerosol collected over the Atlantic Ocean. Marine Chemistry 98 (1), 43–58.

Bell, J., Betts, J., Boyle, E., 2002. MITESS: a moored in situ trace element serial sampler for deep-sea moorings. Deep-Sea Research I 49 (11), 2103–2118.

Blain, S., Quéguiner, B., Armand, L., Belviso, Bombled, B., Bopp, L., Bowie, A., Brunet, C., Brussaard, C., Carlotti, F., Christaki, U., Corbière, A., Durand, I., Ebersbach, F., Fuda, J.-L., Garcia, N., Gerringa, L., Griffiths, B., Guigue, C., Guillerm, C., Jacquet, S., Jeandel, C., Laan, P., Lefèvre, D., Lo Monaco, C., Malits, A., Mosseri, J., Obernosterer, I., Park, Y.-H., Picheral, M., Pondaven, P., Remenyi, T., Sandroni, V., Sarthou, G., Savoye, N., Scouarnec, N., Souhaut, M., Thuiller, D., Timmermans, K.R., Trull, T., Uitz, J., van Beek, P., Veldhuis, M., Vincent, D., Viollier, D., Vong, L., Wagener, T., 2007. Effect of natural iron fertilization on carbon sequestration in the Southern Ocean. Nature 446 (7139), 1070–1074.

Blain, S., Sarthou, G., Laan, P., 2008a. Distribution of dissolved iron during the natural iron-fertilization experiment KEOPS (Kerguelen Plateau, Southern Ocean). Deep-Sea Research II 55 (5–7), 594–605.

Blain, S., Quéguiner, B., Trull, T., 2008b. The natural iron fertilization experiment KEOPS (KErguelen Ocean and Plateau compared Study): an overview. Deep-Sea Research II 55 (5–7), 559–565.

Boström, K., Peterson, M.N.A., 1969. The origin of aluminum-poor ferromanganoan sediments in areas of high heat flow on the East Pacific Rise. Marine Geology 7 (5), 427–447.

Bowie, A.R., Achterberg, E.P., Blain, S., Boye, M., Croot, P.L., De Baar, H.J.W., Laan, P., Sarthou, G., Worsfold, P.J., 2003. Shipboard analytical intercomparison of dissolved iron in surface waters along a north–south transect of the Atlantic Ocean. Marine Chemistry 84 (1–2), 19–34.

Bowie, A.R., Achterberg, E.P., Croot, P.L., De Baar, H.J.W., Laan, P., Moffett, J.W., Ussher, S., Worsfold, P.J., 2006. A community-wide intercomparison exercise for the determination of dissolved iron in seawater. Marine Chemistry 98 (1), 81–99.

Boyd, P.W., Jickells, T., Law, C.S., Blain, S., Boyle, E.A., Buesseler, K.O., Coale, K.H., Cullen, J.J., De Baar, H.J.W., Follows, M., Harvey, M., Lancelot, C., Levasseur, M., Owens, N.J.P., Pollard, R., Rivkin, R.B., Sarmiento, J., Schoemann, V., Smetacek, V., Takeda, V., Tsuda, A., Turner, S., Watson, A., 2007. Mesoscale iron enrichment experiments 1993–2005: synthesis and future directions. Science 315, 612–617.

Boye, M., van den Berg, C.M.G., De Jong, J.T.M., Leach, H., Croot, P., De Baar, H.J.W., 2001. Organic complexation of iron in the Southern Ocean. Deep-Sea Research I 48 (6), 1477–1497.

Boyle, E.A., Bergquist, B.A., Kayser, R.A., Mahowald, N., 2005. Iron, manganese, and lead at Hawaii Ocean Time-series station ALOHA: temporal variability and an intermediate water hydrothermal plume. Geochimica et Cosmochimica Acta 69 (4), 933–952.

Buma, A.G.J., de Baar, H.J.W., Nolting, R.F., van Bennekom, A.J., 1991. Metal enrichment experiments in the Weddell-Scotia Seas: effects of iron and manganese on various plankton communities. Limnology and Oceanography 36 (8), 1865–1878.

Cassar, N., Bender, M.L., Barnett, B.A., Fan, S., Moxim, W.J., Levy II, H., Tilbrook, B., 2007. The Southern Ocean biological response to aeolian iron deposition. Science 317, 1067–1070.

Coale, K.H., Johnson, K.S., Fitzwater, S.E., Gordon, R.M., Tanner, S., Chavez, F.P., et al., 1996. A massive phytoplankton bloom induced by an ecosystem-scale iron fertilization experiment in the equatorial Pacific Ocean. Nature 383, 495–501.

Coale, K.H., Gordon, R.M., Wang, X., 2005. The distribution and behavior of dissolved and particulate iron and zinc in the Ross Sea and Antarctic Circumpolar current along 170°W. Deep-Sea Research I 52, 295–318.

Croot, P.L., Andersson, K., Öztürk, M., Turner, D.R., 2004. The distribution and speciation of iron along 6°E in the Southern Ocean. Deep-Sea Research II 51 (22–24), 2857–2879.

Croot, P.L., Baars, O., Streu, P., 2011. The distribution of dissolved zinc in the Atlantic sector of the Southern Ocean. Deep-Sea Research II 58, 2707–2719.

De Baar, H.J.W., Buma, A.G.J., Nolting, R.F., Cadée, G.C., Jacques, G., Tréguer, P.J., 1990. On iron limitation of the Southern Ocean: experimental observations in the Weddell and Scotia Seas. Marine Ecology-Progress Series 65, 105–122.

De Baar, H.J.W., De Jong, J.T.M., Bakker, D.C.E., Löscher, B., Veth, C., Bathman, U., Smetacek, V., 1995. Importance of iron for plankton blooms and carbon dioxide drawdown in the Southern Ocean. Nature 373 (6513), 412–415.

De Baar, H.J.W., van Leeuwe, M.A., Scharek, R.A., Goeyens, L., Bakker, K., Fritsche, P., 1997. Nutrient anomalies *in Fragilariopsis kerguelensis* blooms, iron deficiency and the nitrate/phosphate ratio (A.C. Redfield) of the Antarctic Ocean. Deep-Sea Research II 44 (1/2), 229–260.

De Baar, H.J.W., Boyd, P.M., 2000. The role of iron in plankton ecology and carbon dioxide transfer of the global oceans. In: Hanson, R.B., Ducklow, H.W., Field, J.G. (Eds.), The Dynamic Ocean Carbon Cycle: A Midterm Synthesis of the Joint Global Ocean Flux Study, International Geosphere Biosphere Programme Book Series, vol. 5. Cambridge University Press, pp. 61–140 (Chapter 4) ISBN:0 521 65603 6.

De Baar, H.J.W., de Jong, J.T.M., 2001. Distributions, sources and sinks of iron in seawater. In: Turner, D., Hunter, K.A. (Eds.), Biogeochemistry of Iron in Seawater, IUPAC Book Series on Analytical and Physical Chemistry of Environmental Systems, vol. 7, 2001, pp. 123–254 (Chapter 5).

De Baar, H.J.W., De La Roche, J., 2003. Metals in the oceans; evolution, biology and global change. In: Lamy, F., Wefer, G. (Eds.), Marine Scientific Frontiers for Europe. Springer-Verlag, Berlin, pp. 79–105.

De Baar, H.J.W., Boyd, P.W., Coale, K.H., Landry, M.R., Tsuda, A.K., Assmy, P., Bakker, D.C.E., Bozec, Y., Barber, R.T., Brzezinski, M.A., Buesseler, K.O., Boyé, M., Croot, P.L., Gervais, R.F., Gorbunov, M.Y., Harrison, P.J., Hiscock, W.T., Laan, P., Lancelot, C., Law, C., Levasseur, M., Marchetti, A., Millero, F.J., Nishioka, J., Nojiri, Y.van Oijen, T., Riebesell, U., Rijkenberg, M.J.A., Saito, H., Takeda, S., Timmermans, K.R., Veldhuis, M.J.W., Waite, A.M.,2005. Synthesis of iron fertilization experiments: from the Iron Age in the age of enlightenmentJournal of Geophysical Research110C09S1610.1029/2004JC002601.

De Baar, H.J.W., Timmermans, K.R., Laan, P., De Porto, H.H., Ober, S., Blom, J.J., Bakker, M.C., Schilling, J., Sarthou, G., Smit, M.G., Klunder, M., 2008. Titan: a new facility for ultraclean sampling of trace elements and isotopes in the deep oceans in the international Geotraces program. Marine Chemistry 111 (1–2), 4–21.

De Jong, J.T.M., Den Das, J., Bathmann, U., Stoll, M.H.C., Kattner, G., Nolting, R.F., De Baar, H.J.W., 1998. Dissolved iron at subnanomolar levels in the Southern Ocean as determined by ship-board analysis. Analytica Chimica Acta 377, 113–124.

Duce, R.A., Tindale, N.W., 1991. Atmospheric transport of iron and its deposition in the ocean. Limnology and Oceanography 36, 1715–1726.

Draxler, R.R., Rolph, G.D., 2003. HYSPLIT (HYbrid Single-Particle Lagrangian Integrated Trajectory) model access via NOAA ARL READY. NOAA Air Resources Laboratory, Silver Spring, MD. Available from: 〈http://www.arl.noaa.gov/ready/hysplit4.htSMLS〉.

Edwards, R., Sedwick, P., Morgan, V., Boutron, C.F., Hong, R., 1998. Iron in ice cores from Law Dome, East Antarctica: implications for past deposition of aerosol iron. Annals of Glaciaology 27, 365–370.

Edwards, R., Sedwick, P., 2001. Iron in East Antarctic snow; implication for atmospheric iron deposition and algal production in Antarctic waters. Geophysical Research Letters 28 (20), 3907–3910.

Eicken, H., 1992. Salinity profiles of Antarctic Sea Ice: field data and model results. Journal of Geophysical Research 97 (10), 15545–15557.

Elrod, V.A., Berelson, W.M., Coale, K.H., Johnson, K.S., 2004. The flux of iron from continental shelf sediments: amissing source for global budgets. Geophysical Research Letters 31, L12307. doi:10.1029/2004GL020216.

Froelich, P.N., Klinkhammer, G.P., Bender, M.L., Luedtke, N.A., Heath, G.R., Cullen, D., Dauphin, P., Hammond, D., Hartman, B., Maynard, V., 1979. Early oxidation of organic matter in pelagic sediments of the eastern equatorial Atlantic: suboxic diagenesis. Geochimica et Cosmochimica Acta 43 (7), 1075–1090.

Fung, I.Y., Meyn, S.K., Tegen, I., Doney, S.C., John, S.G., Bisshop, J.K.G., 2000. Iron supply and demand in the upper ocean. Global Biogeochemical Cycles 14 (1), 281–295.

Garrity, C., Romseier, R.O., Peinert, R., Kern, S., Fisher, G., 2005. Water-column particulated organic carbon modeled fluxes in the ice-frequented Southern Ocean. Journal of Marine Systems 56, 133–149.

Gladyshev, S., Arhan, M., Sokov, A., Speich, S., 2008. A hydrographic section from South Africa to the southern limit of the Antarctic Circumpolar Current at the Greenwich meridian. Deep-Sea Research I 55 (10), 1284–1303.

Gordon, A.L., Taylor,H.W., Georgi,D.T., 1977. Antarctic oceanography zonation. In: Proceedings of SCOR/SCAR Polar Oceans Conference, Montreal, Canada,

May 5–11, 1974,. Dunbar, M.J.(Ed.), Arctic Institution of North America. McGill University, Montreal.
Gran, H.H., 1931. On the conditions for the production of plankton in the sea. Rapports et Proces-verbaux Conseil Permenant d'Exploration de la Mer 75, 37–46.
Gregg, W.W., Ginoux, P., Schopf, P.S., Casey, N.W., 2003. Phytoplankton and iron: validation of a global three-dimensional ocean biogeochemical model. Deep-Sea Research I 50 (22–26), 3143–3169.
Han, Q., Moore, J.K., Zender, C., Measures, C., Hydes, D., 2008. Constraining oceanic dust deposition using surface ocean dissolved Al. Global Biogeochemical Cycles 22, GB2003. doi:10.1029/2007GB002975.
Hand, J.L., Mahowald, N.M., Chen, Y., Siefert, R.L., Luo, C., Subramaniam, A., Fung, I., 1999. Estimates of atmospheric-processed soluble iron from observations and a global mineral aerosol model: biogeochemical implications. Journal of Geophysical Research 109, D17205. doi:10.1029/2004JD004574.
Hart, T.J., 1934. On the phytoplankton of the Southwest Atlantic and the Bellingshausen Sea, 1929–1931. Discovery Reports 8, 1–68.
Hart, T.J., 1942. Phytoplankton periodicity in Antarctic surface waters. Discovery Reports 21, 261–365.
Hoppema, M., Middag, R., De Baar, H.J.W., Fahrbach, E., van Weerlee, E., Thomas, H., 2007. Whole season net community production in the Weddell Sea. Polar Biology 31, 101–111.
Hutchins, D.A., Bruland, K.W., 1994. Grazer mediated regeneration and assimilation of Fe, Zn and Mn from planktonic prey. Marine Ecology-Progress Series 110, 259–269.
Jickells, T.D., Spokes, L.J., 2001. Atmospheric iron inputs to the oceans. In: Turner, D., Hunter, K.A. (Eds.), Biogeochemistry of Iron in Seawater, IUPAC Book Series on Analytical and Physical Chemistry of Environmental Systems, vol. 7, 2001, pp. 85–122 (Chapter 4).
Jickells, T.D., An, T.S., Andersen, K.K., Baker, A.R., Bergametti, G., Brooks, N., Cao, J.J., Boyd, P.W., Duce, R.A., Hunter, K.A., Kawahata, H., Kubilay, N., laRoche, J., Liss, P.S., Mahowald, N., Prospero, J.M., Ridgwell, A.J., Tegen, I., Torres, R., 2005. Global iron connections between desert dust, ocean biogeochemistry and climate. Science 308(67), 67–71.
Johnson, K.S., Boyle, E., Bruland, K., Measures, C., Moffett, J., Aquilarislas, A., Barbeau, K., Cai, Y., Chase, Z., Cullen, J., Doi, T., Elrod, V., Fitzwater, S., Gordon, M., King, A., Laan, P., Laglera-Baquer, L., Landing, W., Lohan, M., Mendez, J., Milne, A., Obata, H., Ossiander, L., Plant, J., Sarthou, G., Sedwick, P., Smith, G.J., Sohst, B., Tanner, S., Van Den Berg, S., Wu, J., 2007. Developing standards for dissolved iron in seawater. Eos Transactions of the AGU 88 (11), 131.
Klatt, O., Fahrbach, E., Hoppema, M., Rohardt, G., 2005. The transport of the Weddell Gyre across the Prime Meridian. Deep-Sea Research II 52 (3–4), 513–528.
Klinkhammer, G.P., Chin, C.S., Keller, R.A., Dählman, A., Sahling, H., Sarthou, G., Petersen, S., Smith, F., Wilson, C., 2001. Discovery of new hydrothermal vent sites in Bransfield Strait, Antarctica. Earth and Planetary Science Letters 193 (3–4), 395–407.
Klunder, M.B., Laan, P., Middag, R., Thuroczy, C.E., De Baar, H.J.W. Very low dissolved Fe in Arctic Deep Waters, despite hydrothermal and shelf sources, in preparation.
Laës, A., Blain, S., Laan, P., Achterberg, E.P., Sarthou, G., De Baar, H.J.W., 2003. Deep dissolved iron profiles in the eastern North Atlantic in relation to water masses. Geophysical Research Letters 30 (17), 1–3.
Laës, A., Baker, A.R., Kramer, J., Laan, P., Ussher, S., Achterberg, E.P., De Baar, H.J.W., Timmermans, K.R., Blain, S., 2007. Sources and transport of dissolved iron and manganese along the continental margin of the Bay of Biscay. Biogeosciences 4, 181–194.
Lai, X., Norisuye, K., Mikata, M., Minami, T., Bowie, A.R., Sohrin, Y., 2008. Spatial and temporal distribution of Fe, Ni, Cu and Pb aloong 140*E in the Southern Ocean during austral summer 2001/02. Marine Chemistry 111, 171–183.
Lam, P.J., Bishop, J.K.B., Henning, C.C., Marcus, M.A., Waychunas, G.A., Fung, I., 2006. Wintertime phytoplankton bloom in the subarctic Pacific supported by continental margin iron. Global Biogeochemical Cycles 20, GB 1006. doi:10.1029/2005GB002557.
Lancelot, C., de Montety, A., Goosse, H., Becquevort, S., Schoemann, V., Pasquer, B., Vancoppenolle, M., 2009. Spatial distribution of the iron supply to phytoplankton in the Southern Ocean: a model study. Biogeosciences Discussions 6, 4919–4962.
Lannuzel, D., Schoemann, V., De Jong, J.T.M., Chou, L., Delille, B., Becquevort, S., Tison, J.-L., 2008. Iron study during a time series in the western Weddell pack ice. Marine Chemistry 108 (1–2), 85–95.
Löscher, B.M., De Baar, H.J.W., De Jong, J.T.M., Veth, C., Dehairs, F., 1997. The distribution of Fe in the Antarctic circumpolar current. Deep-Sea Research II 44 (1–2), 143–187.
Mackie, D.S., Peat, J.M., McTainsh, G.H., Boyd, P.W., Hunter, K.A., 2006. Soil abrasion and eolian dust production: implications for iron partitioning and solubility. Geochemistry Geophysics Geosystems 7, 12. doi:10.1029/2006GL026557.
Mahowald, N., Kohfeld, K., Hansson, M., Balkanski, Y., Harrison, S.P., Prentice, I.C., Schulz, M., Rodhe, H., 1999. Dust sources and deposition during the last glacial maximum and current climate: a comparison of model results with paleodata from ice cores and marine sediments. Journal of Geophysical Research 104 (D13), 15.895–15.916.
Mahowald, N.M., Baker, A.R., Bergametti, G., Brooks, N., Duce, R.A., Jickells, T.D., Kubilay, N., Prospero, J.M., Tegen, I., 2005. Atmospheric global dust cycle and iron inputs to the ocean. Global Biogeochemical Cycles 19 (4025). doi:10.1029/2004GB002402.
Martin, J.H., Fitzwater, S.E., 1988. Iron deficiency limits phytoplankton growth in the north-east Pacific subarctic. Nature 331 (6154), 341–343.
Measures, C.I., Vink, S., 2001. Dissolved Fe in the upper waters of the Pacific sector of the Southern Ocean. Deep-Sea Research II 48 (19–20), 3913–3941.
Measures, C.I., Landing, W.M., Brown, M.T., Buck, C.S., 2008. High-resolution Al and Fe data from the Atlantic Ocean CLIVAR-CO_2 Repeat Hydrography A16N transect; extensive linkages between atmospheric dust and upper ocean geochemistry. Global Biogeochemical Cycles 22, GB 1005. doi:10.1029/2007/GB003042.
Middag, R., De Baar, H.J.W., Laan, P., Bakker, K., 2009. Dissolved aluminium and the silicon cycle in the Arctic Ocean. Marine Chemistry 115, 176–195.
Middag, R., De Baar, H.J.W., Laan, P., Cai, P., van Ooijen, J.C., 2011a. Dissolved manganese in the Southern Ocean. Deep-Sea Research II 58, 2661–2677.
Middag, R., van Slooten, C., De Baar, H.J.W., Laan, P., 2011b. Dissolved aluminium in the Southern Ocean. Deep-Sea Research II 58, 2647–2660.
Moore, J.K., Braucher, O., 2008. Sedimentary and mineral dust sources of dissolved iron to the world ocean. Biogeosciences 5 (3), 631–656.
Neven, I., Stefels, J., De Baar, H.J.W., Elzenga, T., 2011. High adaptability in inorganic carbon uptake by Southern Ocean phytoplankton in response to ambient CO_2. Deep-Sea Research II 58, 2636–2646.
Nishioka, J., Takeda, S., De Baar, H.J.W., Croot, P.L., Boye, M., Laan, P., Timmermans, K.R., 2005. Changes in the concentration of iron in different size fractions during an iron enrichment experiment in the open Southern Ocean. Marine Chemistry 95 (1–2), 51–63.
Parekh, P., Follows, M.J., Boyle, E., 2004. Modeling the global ocean iron cycle. Global Biogeochemical Cycles 19, GB 2020. doi:10.1029/2004GB002280.
Park, Y.H., Charriaud, E., Fieux, M., 1998. Thermohaline structure of the Antarctic Surface Water/Winter Water in the Indian sector of the Southern Ocean. Journal of Marine Systems 17 (1–4), 5–23.
Planquette, H., Statham, P.J., Fones, G.J., Charette, M.A., Moore, C.M., Salter, I., Nédélec, F.H., Taylor, S.L., French, M., Baker, A.R., Mahowald, N., Jickells, T.M., 2007. Dissolved iron in the vicinity of the Crozet Islands, Southern Ocean. Deep-Sea Research II 54 (18–20), 1999–2019.
Pollard, R.T., et al., 2009. Southern Ocean deep-water carbon export enhanced by natural iron fertilization. Nature 457 (7229), 577–580.
Rutgers van der Loeff, M., Cai, P., Stimac, I., Bracher, A., Middag, R., Klunder, M.B., van Heuven, S., 2011. ^{234}Th in surface waters: distribution of particle export flux across the Antarctic Circumpolar Current and in the Weddell Sea during the GEOTRACES expedition ZERO and DRAKE. Deep-Sea Research II 58, 2749–2766.
Sarthou, G., Baker, A.R., Blain, S., Achterberg, E.P., Boye, M., Bowie, A., Croot, P.L., Laan, P., De Baar, H.J.W., Jickells, T.M., Worsfold, P.F., 2003. Atmospheric iron deposition and sea-surface dissolved iron concentrations in the eastern Atlantic Ocean. Deep-Sea Research I 50 (10–11), 1339–1352.
Sarthou, G., Timmermans, K.R., Blain, S., Tréguer, P., 2005. Growth physiology and fate of diatoms in the ocean: a review. Journal of Sea Research 53 (1–2), 25–42.
Sarthou, G., Vincent, D., Christaki, U., Obernosterer, I., Timmermans, K.R., Brussaard, C.P.D., 2008. The fate of biogenic iron during a phytoplankton bloom induced by natural fertilisation: impact of copepod grazing. Deep-Sea Research II 55 (5–7), 734–751.
Schlitzer, R., 2009. Ocean Data View. Available from: 〈http://www.odv.awi.de〉.
Sedwick, P.N., Edwards, P.R., Mackey, D.J., Griffiths, F.B., Parslow, J.S., 1997. Iron and manganese in surface waters of the Australian subantarctic region. Deep-Sea Research I 44, 1239–1253.
Sedwick, P.N., Bowie, A.R., Trull, T.W., 2008. Dissolved iron in the Australian sector of the Southern Ocean (CLIVAR SR3 section); Meridional and seasonal trends. Deep-Sea Research I 55, 911–925.
Sohrin, Y., Iwamoto, S., Matsui, M., Obata, H., Nakayama, E., Suzuki, K., Handa, N., Ishii, H., 2000. The distribution of Fe in the Australian Section of the Southern Ocean. Deep-Sea Research I 47 (1), 55–84.
Sunda, W.G., Huntsman, S.A., 1997. Interrelated influence of iron, light and cell size on marine phytoplankton growth. Nature 390, 389–392. doi:10.1038/37093.
Sunda, W.G., 2001. Bioavailability and bioaccumulation of iron in the seawater. In: Turner, D., Hunter, K.A. (Eds.), Biogeochemistry of Iron in Seawater, IUPAC Book Series on Analytical and Physical Chemistry of Environmental Systems, vol. 7, 2001, pp. 41–85 (Chapter 3).
Tagliabue, A., Bopp, L., Aumont, O., 2009. Evaluating the importance of atmospheric and sedimentary iron sources to Southern Ocean biogeochemistry. Geophysical Research Letters 36, L13601. doi:10.1029/2009GL038914.
Taylor, S.R., McLennan, S.M., 1985. The Continental Crust: Its Composition and Evolution. Blackwell.
Thuróczy, C.-E., Gerringa, L.J.A., Klunder, M.B., Laan, P., De Baar, H.J.W, 2011. Observation of consistent trends in the organic complexation of dissolved iron in the Atlantic Sector of the Southern Ocean. Deep-Sea Research 58, 2695–2706.
Tovar-Sanchez, A., Duarte, C.M., Hernández-Léon, S., Saňudo-Wilhelmy, S.A., 2007. Krill as a central node for iron cycling in the Southern Ocean. Geophysical Research Letters 34, L61101.
Twining, B.S., Baines, S.B., Fisher, N.S., Landry, M.R., 2004. Cellular iron contents of plankton during the Southern Ocean Iron Experiment (SOFeX). Deep-Sea Research I 51, 1827–1850.
Veth, C., Peeken, I., Scharek, R., 1997. Physical anatomy of fronts and surface waters in the ACC near the 6°W meridian during austral spring 1992. Deep-Sea Research II 44 (1–2), 23–49.

Walter, H.J., Rutgers van der Loeff, M.M., Höltzen, H., Bathmann, U., 2000. Reduced scavenging of 230Th in the Weddell Sea: implications for paleoceanographic reconstructions in the South Atlantic. Deep-Sea Research I 47 (7), 1369–1387.
Wedepohl, K.H., 1995. The composition of the continental crust. Geochimica et Cosmochimca Acta 59 (7), 1217–1232.
Wolff, E.W., Hall, E.J., Mulvaney, R., Pasteur, E.C., Wagenbush, D., Legrand, M., 1989. Relationship between chemistry of air, fresh snow and firn cores for aerosol species in coastal Antarctica. Journal of Geophysical Research 103, D9. doi:10.1029/97JD02613.
Worby, A.P., Geiger, C.A., Paget, M.J., Van Woert, M.L., Ackley, S.F., DeLiberty, T.L., 2008. Thickness distribution of Antarctic sea ice. Journal of Geophysical Research 113, C05S92. doi:10.1029/2007JC004254.
Wu, J., Boyle, E., Sunda, W., Wen, L.-S., 2001. Soluble and colloidal iron in the oligotrophic North Atlantic and North Pacific. Science 293, 847–849.